Thermal Measurement of Turbulent Wall Shear Stress Fluctuations: Tackling the Effects of Substrate Heat Conduction

by

Elsa Assadian
B.Sc., University of Semnan, 2007

A Thesis Submitted in Partial Fulfillment
of the Requirements for the Degree of

MASTER OF APPLIED SCIENCES

in the Department of Mechanical Engineering

Supervisory Committee

Thermal Measurement of Turbulent Wall Shear Stress Fluctuations: Tackling the Effects of Substrate Heat Conduction

by

Elsa Assadian
B.Sc., University of Semnan, 2007

Supervisory Committee

Dr. Rustom B. Bhiladvala, (Department of Mechanical Engineering)
Supervisor

Dr. Andrew Rowe, (Department of Mechanical Engineering)
Departmental Member

Abstract

Supervisory Committee

Dr. Rustom B. Bhiladvala, (Department of Mechanical Engineering)
Supervisor
Dr. Andrew Rowe, (Department of Mechanical Engineering)
Departmental Member

This thesis presents a computational analysis of multi-element guard-heated sensors designed to overcome the most severe limitation of conventional thermal sensors for wall shear stress (WSS) measurement in turbulent flows –that of indirect heat conduction through the substrate. The objectives of this thesis are the study of guard-heated sensors {i} to quantify the reduction, over conventional single-element sensors, of substrate heat conduction losses and resultant errors over a range of applied shear and {ii} to examine a range of values of guard heater geometric parameters, in two common fluids, air and water and identify the best designs.

Wall-turbulence, the turbulent flow in the vicinity of solid boundaries, has proved difficult to model accurately, due to the lack of accurate WSS measurements. Examples of areas of impact are drag force reduction on transport vehicles in land, sea, air, which today largely translate to reduced fossil fuel use and dependence; aerodynamic noise and control for flight and for wind energy conversion; atmospheric and oceanic transport studies for weather, climate and for pollutant transport; riverbank erosion.

Constant-temperature anemometry with MEMS devices, flush-mounted hot-film thermal sensors, is non-intrusive, affords the best temporal resolution and is well-established. However, these hot-film probes suffer from unwanted heat transport to the fluid through the substrate, with errors and nonlinearity large enough to overwhelm quantitative utility of the data. Microfabrication techniques have enabled multi-element guard-heated prototypes to be fabricated. Our results show that errors in sensing-element signals, contributing to spectral distortion, are sensitive to sensor location within the guard heater. These errors can be reduced to below 1% of the signal with proper location of the sensor. Guard heating also reduces the large variation in spatial averaging due to substrate conduction. This makes them suitable for turbulent flows with a large range of fluctuations.

Table of Contents

List of Tables

List of Figures

Nomenclature

Nomenclature: Latin

E	voltage
h	heart transfer coefficient
I	currant
K	thermal conductivity
L	streamwise sensor length
L_{eq}	equivalent sensor length
q	heat flux
q_t	total heat flux
Q	heat transfer
R	electrical resistance
s_x	streamwise velocity gradient
T	temperature
ΔT	temperature gradient
t	time
t^*	dimensionless time
W	spanwise sensor length
x	streamwise distance
x^*	dimensionless streamwise distance
y	Normal direction distance
y^*	dimensionless normal distance
z	spanwise distance
z^*	dimensionless spanwise distance

Subscript:

F	fluid
S	substrate
d	direct
I	indirect
Iu	upstream indirect
Id	downstream indirect

Abbreviation:

WSS	wall shear stress
PDF	Probability density function
Nu	Nusselt number ($^{hL}/_{k_f}$)
Nu_t	total Nusselt number
Pe	Peclet number ($\frac{sL^2}{\alpha_f}$)

Nomenclature: Greek

α	thermal diffusivity
δ_t	thermal boundary layer thickness
θ	dimensionless temperature
ρ	density
τ_w	wall shear stress
ω	frequency
ω^*	non-dimensional frequency ($\frac{\omega L^2}{\alpha_f}$)

Acknowledgments

The support, patience and eagerness of those around me were instrumental in making the completion of this thesis a reality. I regret that it is only possible to thank a fraction of these people here.

Above all, I would like to give a special thanks to my supervisor, Dr. Rustom Bhiladvala, for having enough faith in my abilities. Dr. Bhiladvala's dedication and encouragement allowed me to achieve my goals, and he was always available to assist me whenever I needed guidance. I was able to learn much from his unsurpassed passion and knowledge. Without Dr. Bhiladvala's selfless devotion to me, this thesis would not have been possible.

Moral support and technical advice of my officemates, Tom Burdyny, Jean Duquette, and Oliver Campbell, and friends, Nima Moghimian, Mahshid Sam, Ali Etrati, Nasser Yasrebi, Nima Khadem Mohtaram, Geoffrey Lacouvee, Jesse Coelho, and Michael Shives, helped me to pursue my research. They always encouraged me in the times I felt overwhelmed.

Last, I would like to offer a big thank you to my mother, Roya, and father, Hassan, both who have been a source of inspiration in my life. My father has always taught me to reach for the sky, and to be the best in whatever I chose to pursue in life. My mother provided me with guidance and love at times when it was most needed. A special thanks to my sister, Poroushat, and brother, Hooman, who offered me their unequivocal support, love and laughs.

Dedication

To my beloved parents

1. Introduction

1.1. Overview

A viscous fluid flowing past a solid boundary (or wall) exerts a stress on the boundary. Pressure is the wall-normal component of the stress and the two components parallel to the plane of the wall constitute the wall shear stress (WSS), as shown in Figure 1-1. In turbulent flows, the WSS is a fluctuating quantity in which large fluctuations play a more significant role than for the velocity field.
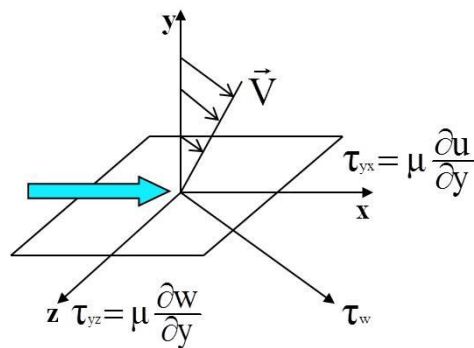
Figure 1-1- Wall shear stress and velocity

For all Newtonian fluids in laminar flow, shear stress is proportional to the velocity gradient and dynamic viscosity of the fluid (μ). For a flow with mean flow direction along x, the two components of shear stress in Fig. 1.1, τ_{yx} and τ_{yz} are known as the streamwise and spanwise stress, terms from aeronautics denoting mean flow direction and direction along wing span, respectively. Most flows in nature and technology are turbulent flows —a state characterized by apparent disorder, three-dimensional fluctuations and dissipation and mixing. Particularly for these flows, the wall shear stress has been very difficult to measure, in spite of several measurement attempts by different techniques, over several decades. Why has this information been so strongly sought?

1.1.1. Applications of wall shear stress measurement

Knowledge of WSS is necessary for a workably accurate determination of heat, mass and momentum transport over a range of turbulent flows. Accurate measurement of WSS in turbulent flow is needed to understand and model drag force reduction, fluid energy dissipation, mixing and flow separation. With drag reduction, the amount of fuel consumption, pollutant and CO_2 emissions would be greatly reduced in transport vehicles. As an example, more efficient design of aircraft or cargo ships known as the biggest fuel consumers saves energy and cost.

In many engineering applications, measuring the distribution of WSS, which is a direct measure of the fluid forces on the solid surface, is still one of the main interests that needs to be investigated. As an illustration, wind turbine performance could be improved remarkably if we can change the blade shape according to the WSS distribution measured at locations on the blade surface, rather than the wind speed measured at a distance from the turbine blades. By this means, not only could the energy conversion efficiency of the system increase, but forces on the structure contributing to fatigue or extreme-load failures could also be reduced. As another example, knowledge of wall shear stress fluctuation distribution in river bank erosion, which is a substantial issue for civil engineers, is more important than the mean value of wall shear stress. Calculations based on the mean wall shear stress, or on a Gaussian distribution of fluctuations, under-predicts erosion rates, showing that the perturbation of transport due to strong fluctuations is significant, even though they occur rarely.

From a scientific point of view, much can be learned about the unsteady structure of turbulent flow from WSS measurements. It helps us understand relationships in wall

turbulence such as between local velocity and energy dissipation. In this case, the correlation between velocity and wall shear stress needs to be quantified. In addition, proposal and validation of near-wall turbulence models require WSS measurement. Strong fluctuations with respect to the mean are more prevalent in the turbulent WSS field than the velocity field. A few experiments and direct numerical simulation (DNS) results at low Reynolds number, show that the probability density function (PDF) of WSS decays more slowly than the velocity PDF, which appears at first sight to be closer to a Gaussian. The strongly non-Gaussian PDF for WSS, indicates the existence of a distinct structure of the near-wall flow. Several probability density functions have been reported by using different methods. S. Grosse *et al.* reported PDFs of streamwise and spanwise shear stress by applying micro-pillar sensors MPS[3] [1]. Spatial distribution of shear stress shows the association of high spanwise wall shear stress to streamwise shear stress and wall normal momentum transfer. This relation can be explained by existence of eddies close to the wall which bring high-speed fluid away from the wall to the low-speed region near the wall. The following figure includes the PDF of streamwise WSS fluctuations reported by S. Grosse *et al.* as well as other groups.
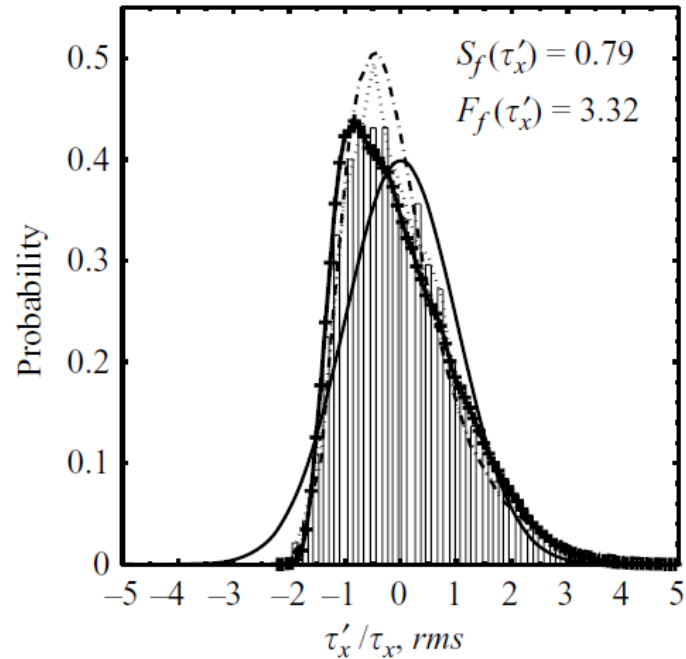
Figure 1-2- PDF of the streamwise wall-shear stress fluctuations, −+− results reposted by Grosse *et al*. (2009) at $Re_{H,b} = 15,400$, −.− results reported by Miyagi *et al*. (2000) at $Re_{H,cl} = 17,600$, bar chart reported by Obi *et al*. (1996) at $Re_{H,cl} = 6,600$, … results reported by Sheng *et al*. (2008) at $Re_{H,cl} = 100,000$, and − shows Gaussian distribution [1].

This figure shows asymmetry typical of streamwise WSS PDFs. The long heavy tail of this PDF indicates slower decay of this curve, showing larger fluctuations occur more frequently than for a Gaussian distribution. This behavior of the PDF can be translated directly to the practical example we mentioned earlier -river bank erosion can happen at higher rates as a result of large and infrequent fluctuations, compared to small and frequent fluctuations.

Another interesting application of skin-friction measurement is the potential use for active control for skin friction drag reduction [2]. In active control, the state of the system is continuously monitored by a sensor or arrays of sensors at various locations. A control system uses input from the sensors to drive actuators that modify the fluctuations

in the velocity field with the goal of reducing skin friction drag force. In order to do so, large numbers of small sensors and actuators are typically required. Wall skin friction reduction in many applications, can be done by manipulation of near-wall vortices. Lofdahl *et al.* (1999) reported a 60% reduction of skin-friction using the suction method when implementing reactive control [3]. Iwamoto *et al*. (2005) also reported that near-wall turbulence ($y^+ = 10$) attenuation by using the active feedback control method at $Re_\tau = 10^5$ leads to a 35% drag reduction [4]. In addition, by using the active control system in aircraft design, separation can be delayed to prevent stall for improved manoeuvrability. The question that arises here is whether we can control the flow by manipulating large-scale structure away from the wall or whether a detailed understanding of the near-wall instantaneous flow field is necessary.

The difficulty in answering this question is that near-wall structure of turbulent flow as well as its interaction with large-scale structures still requires much to be completely understood. Iwamoto *et al*. (2004) studied quasi-streamwise vortices and the large-scale outer layer interaction by the direct numerical simulation (DNS) method in turbulent channel flow [5]. They reported that the large-scale structures exist at a distance from the wall ($y^+ = 30$) to the center of the channel, while the streaky structures with 100 wall unit spanwise spacing present at ($y^+ < 30$) in $Re_\tau = 1160$. It is thought that turbulent kinetic energy gained by the near-wall small scale vortices from the mean flow is mainly lost by these small near-wall structures, with some being transferred to the large-scale structure by nonlinear interaction. This suggests that the rate of energy dissipation can be influenced mainly by manipulating near-wall structure.

In spite of the strong need to understand the interaction between fluctuations of the WSS and their relationship to the near-wall velocity field in turbulent flows, it has proved extraordinarily difficult to make such measurements with reasonable accuracy over a range of flow conditions. The importance of these measurements is underscored by the fact that several transduction principles have been attempted. These are first reviewed in this thesis. Thermal sensing using microfabricated guard heaters are the subject of this thesis, with the detailed objectives stated below.

1.2. Objectives

New guard-heated thermal WSS sensors to overcome the severe limitations of conventional single–element hot-film sensors are first explained, and then studied numerically in this thesis. The fundamental purpose is to remove large measurement errors in thermal sensing with single-element hot-film probes. To do so, we numerically evaluate new guard-heated thermal sensor designs. The research contributions of this thesis are the establishment of material, geometric and thermal parameters that will allow the guard-heated thermal sensor designs to function without the most significant errors arising from unwanted substrate heat conduction. These are listed below.

- Investigating the influence of solid-to-fluid thermal conductivity ratio on resolution of the conventional sensor.
- Assessment of sensor characteristics by computational heat transfer in water and air flows.
- Comparison of all single–element and guard–heated sensors in terms of error contribution in signals.

- Examining two designs of microfabricated sensors using guard-heaters in a single plane and in two planes, and finding the best geometric parameters to minimize the effects of substrate heat conduction.

- Studying the effect of temperature dependent fluid properties on the sensor performance.

1.3. Thesis organization

This thesis includes five chapters. In this Chapter 1, an introduction was provided, which comprises the motivation for and objectives of the work in the thesis. The roles of WSS sensors in industrial and scientific applications were discussed.

Chapter 2 begins with the necessity of measuring wall shear stress with high resolution sensors in turbulent flows. In the next section, the methods of wall shear stress measurement including direct and indirect methods as well as relative examples are discussed. Several techniques available in literature, more specifically thermal wall shear stress sensors, are reviewed. The pros and cons of this type of sensor, in addition to methods employed to overcome its deficiencies, are also presented.

Chapter 3 provides the principles of thermal wall shear stress sensors. It includes the following: theoretical considerations; governing equations used to model the intended system; and limitations of the probe. This is followed by description and checks of the methods for numerical investigation of a single–element sensor. Two new designs, which are referred to as guard–heated sensors in a plane and guard–heated sensors on two planes, are introduced. Finally, a microfabrication method used to create the guard-heated sensors is described.

Chapter 4 provides results from a series of studies which are related to the designs described in Chapter 3. The performance of single–element sensors and the effect of a conductive substrate on the device is followed by studies of guard–heated sensors on one and two planes. All the probes are mainly analysed in water flow with constant fluid properties. In addition, air and fluids with temperature–dependent properties are also considered. At the end, the effect of substrate thermal conductivity on the sensor is also investigated.

Chapter 5 includes a summary of the main results and conclusions that are the contributions of this thesis work, as well as recommendations for future work.

2. Approaches to wall shear stress fluctuation measurement

2.1. Requirement of high resolution sensors

For measuring turbulent quantities, we should keep in mind that turbulent flow has a large range of fluctuations in space and with time. Therefore, the length and time scale resolution of the sensor should be small enough to avoid spatial and time-averaging errors. Increase in the Reynolds number, Re, in a given flow geometry leads decreases the minimum length and time scale, which needs a sensor with a higher resolution, of the order of the relevant Kolmogorov length and timescales, η and T respectively, given by:

$$\begin{cases} \dfrac{\eta}{\delta} \sim Re_\delta^{-\frac{3}{4}} \\[4mm] \dfrac{Tu}{\delta} \sim Re_\delta^{-1/2} \end{cases} \qquad \text{Eq. 2-1}$$

Reynolds number, $Re_\delta = u\delta/v$, is based on the boundary layer thickness δ, kinematic viscosity v, and the eddy velocity scale u, $(\frac{u}{U} \sim 10^{-2})$ [6]. If we anticipate correlation between the near-wall velocity field and WSS fluctuations, it would be a reasonable goal to require that the WSS sensor have resolution down to the Kolmogorov scale limits.

Many scientists have focused on maximizing the skin-friction sensor resolution and measuring fluctuating shear stress. Among all the available methods, MEMS thermal sensors have some interesting characteristics, which earlier made them the strongest choice for measurement of WSS fluctuations. The feasibility of making microscale thermal sensors with microfabrication techniques promises improvement in the time and

spatial resolution of the device, necessary in dynamic flow measurement. However, as we will show, microfabricated single-element thermal sensors may not be able to properly resolve fluctuations that are several times their size, motivating the new approach in this thesis. A number of different transduction approaches, some under recent development, show the strong interest in this measurement, and there is no clear contender ahead of the others. We review the most significant of these approaches from published literature, below.

2.2. Various types of WSS sensors

Wall shear stress plays a pivotal but poorly described role in the understanding of wall-bounded turbulent flows. The strong need to model turbulence has led to the development of several types of WSS sensors over the past decades, with novel transduction attempts often following new microfabrication technologies that become available. Electrochemical probes, floating element sensors, micropillar sensors, thermal sensors such as hot film and hot wire are some examples. None of these techniques has had complete success in measurement over a wide range of flow Reynolds numbers in different fluids.

In general, all the thermal, mechanical and optical sensors can be categorized into two main groups, direct and indirect, based on their principle of measurement. With the direct method, the parameter measured by the sensor is the local shear stress, using a force transducer. Floating-element sensors flush-mounted with the wall are an example of this method. Pressure is the independent third component of flow force on the wall, and WSS sensors based on the direct method must be designed carefully to be pressure

insensitive. Since shear stress affects other quantities in the fluid, such as heat and mass transfer, it can also be measured by an indirect method -by studying the effect of varying WSS on these quantities. For this, we require that quantities such as heat and mass transfer should be connected to WSS theoretically. We need an empirical correlation (calibration) with a theoretical basis for the functional form. Near-wall hot wires, flush-mounted hot film or electrochemical sensors are examples of indirect methods for WSS measurement. The drawback of indirect sensors is that each probe needs to be calibrated in a flow with known and controllable wall shear stress. Each method may be more suited to a particular application and less to others. Their limitations also cause some errors in measurement which will be discussed in more detail in this thesis.

2.2.1. Floating element

A direct method of fluctuating measurement would be measuring the force on a very small section of the wall. K. G. Winter (1977) [7], and M. Acharya (1985) [6] presented one of the earliest local direct measurement shear stress transducers. The motion of a floating element parallel to the boundary is considered in this device. The amount of displacement of the moving element shows the shear stress magnitude. Since the floating element needs a gap around its perimeter in order to have freedom to move, the effect of flow running under the plate is not ignorable; this under plate flow is not determined in calibration. The parallel alignment of the element with the wall is also crucial. Additional forces on the plate because of sensor misalignment, depressions or protrusion can dominate the sensor response [8]. Vibration and pressure gradient can also cause measurement errors.

A schematic figure of floating elements supported by silicon tethers which act as springs is shown at following figure.
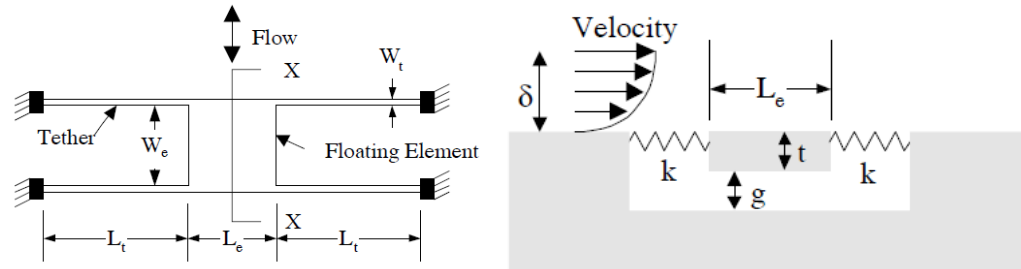
Figure 2-1- (a) Mechanical model of a floating element [9].

In this figure, L_e, W_e, and t represent floating element length, width and thickness. L_t and W_t indicate tether length and width. g is the gap between the substrate and floating element. The relation of sensing element displacement (Δ) and shear stress τ_w is expressed by the Euler-Bernoulli beam theory:

$$\Delta = \tau_w \frac{L_e W_e}{4Et} \left(\frac{L_t}{W_t}\right)^3 \left\{1 + 2\frac{L_t W_t}{L_e W_e}\right\}$$

Eq. 2-2

Note that E is the elastic modulus of the tethers.

M. Sheplak *et al.* (2011) developed a working floating element sensor based on capacitance. They used their sensor for measurement in turbulent boundary layer. The mechanical model is shown in following figure:
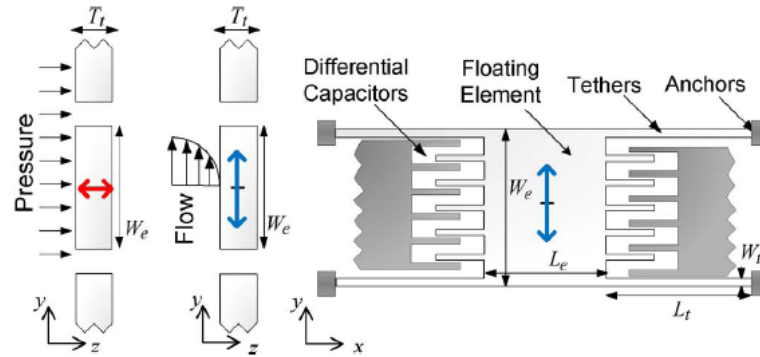
Figure 2-2- The schematic figure of the differential capacitive shear stress sensor [10].

As this figure shows, the floating element is suspended by four compliant tethers. Comb fingers of the floating element on two sides, which act as electrodes are the elements of capacitors along with the fixed fingers in the substrate. When shear stress causes displacement of the moving element, the capacitance will change between the fixed and moving electrodes.

2.2.2. Micro pillar sensors

S. Große *et al*. (2008) studied an indirect shear stress sensor, MPS[3], made using flexible micrometer scale pillars. This method is called indirect, since the shear stress is computed by measuring the near wall velocity gradient in the viscous sublayer and the local surface friction. Pillars are located on the wall. Fluid forces bend the thin cylindrical structure's tip depending on the WSS strength. The structure and mechanical model of the sensor is illustrated in following figures.
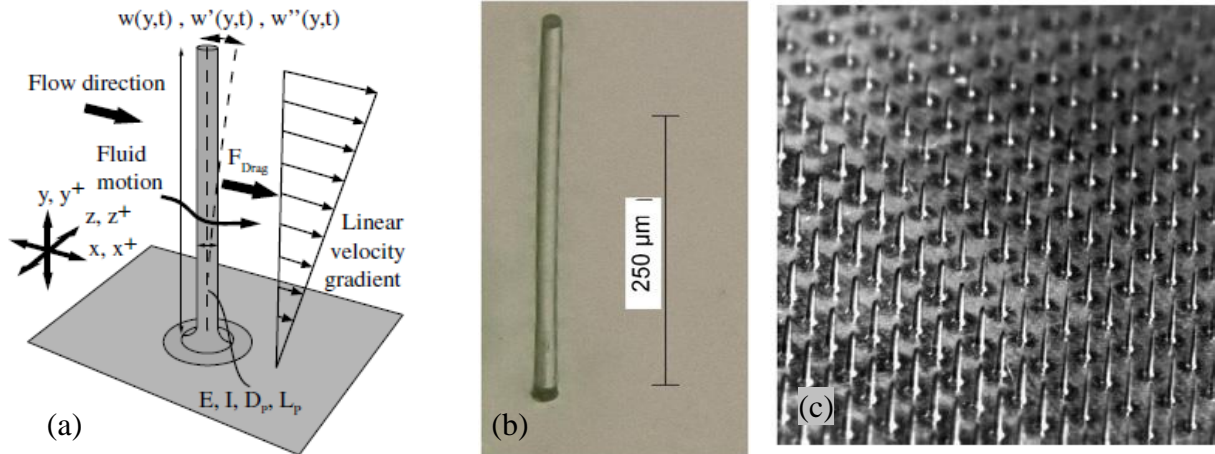
Figure 2-3- (a) Schematic figure of single pillar (b) images of a pillar with 350μm length (c) array of pillars [11].

Their maximum height should not exceed the viscous sublayer thickness where the velocity gradient and WSS have a linear relationship. S. Große and his group have made smaller pillar height than viscous sublayer thickness which is in a range of 80-1000µm for turbulent flows at moderately low Reynolds numbers [11]. They have reported measured values of mean and dynamic wall shear stress; their results showed convincing agreement with the available literature.

High temporal and spatial resolution as well as detecting two-dimensional WSS distribution is a great potential of this sensor, since the symmetric shape of the pillar make it evenly sensitive in both directions parallel to the boundary.

These sensors were used later by Bernardo *et al*. (2011) to investigate the effect of polymers on drag reduction in channel flow. The wall distance of the polymers was controlled by grafting the polymer filament on the micro pillars [12]. The concept of operation is based on micro pillar tip bending, which was detected by a high resolution optical system at frequencies up to 10 kHz. The following equation is used to calculate the amount of deflection:

$$W(L_P) \approx \frac{112}{9} \frac{1}{E} \frac{L_P^5}{D_P^4} \tau$$

<div align="right">**Eq. 2-3**</div>

Note that $W(L_P)$, L_P, and D_P are deflection, height, and diameter of the pillar, respectively. τ is WSS, and E represents Young's modulus.

This equation indicates the high influence of cylinder aspect ratio L_P/D_P on deflection; a high aspect ratio is needed for higher sensitivity of shear stress; however, the length is limited by the viscous sublayer thickness and the spatial averaging error due to applying long micro pillars should be taken into account. The rms (root mean square) value of streamwise fluctuations $(\tau_{x,rms}/\bar{\tau}_x)$ measured by S. Große *et al.* (2008) is approximately 0.39 at Re=10,000 when the pillar height is about 350 μm; It should be noted that the rms value decreases, $\frac{\tau_{x,rms}}{\bar{\tau}_x} = 0.33 - 0.34$, as the Re number increases to Re=20,000 [11]. Deviation of this ratio in comparison to the typical $\frac{\tau_{x,rms}}{\bar{\tau}_x} = 0.4$, can be considered as spatial averaging along the sensor height.

The diameter of each cylinder should be micrometer-scale to decrease the stiffness of the pillars for more sensitivity to fluid forces; more flexibility of the sensors indicates a higher bending angle depending on the shear.

In addition to geometrical quantification, mechanical properties of the sensors such as Young's modulus should be considered in design. Choosing the proper material is a trade off between the high sensor sensitivity and fluctuation strength. Young's modulus suitable for small fluctuations can cause non-linearity of the tip deflection in strong fluctuations. Bernardo *et al.* proved the tip deflection shows a non-linear trend at shear stress higher than 5 Pa; the linear bending theory is valid only up to $\frac{w(L_P)}{L_P} = 0.05 - 0.06$

or with shear stress less than 2 Pa. This fact puts limitation on micro pillar sensor applications.

Tip bending detection by an optical system is another concern, especially when arrays of pillars are used. Bernardo *et al*. have also enhanced the method of bending detection by attaching hollow silver-coated glass spheres on top of the pillars as shown in the following figure:
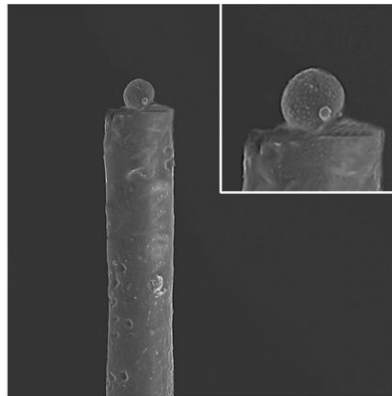
Figure 2-4- Image of a pillar with a reflective hollow sphere taken with a scanning electron microscope (SEM) [12].

The measurement can be done in a wide area using arrays of pillars; however, the presence of the cylinder inside the flow changes the flow pattern in the sublayer, as each sensor is affected by its neighbouring pillars in arrays of pillars. Analysing the flow field using μPIV and streakline visualization of the flow around the pillar showed the flow past the pillars is still in the Stokes regime at various Reynolds numbers based on cylinder diameter; the wakes are presented only to about four times the pillar diameter. Thus the pillars spacing should be higher than this value to avoid the influence of cantilevers on each pillar [12].

In this type of device, the resistance against shear stress such as the internal viscous material damping is an issue which cannot be exactly estimated.

2.2.3. Optical probes

An optical sensor was introduced by U.K. Ayaz [13]. The sensor is made of a dielectric sphere; the available force imposed on the microsphere changes its optical mode. The measurement is done by tracking the shift in optical modes (WGM-whispering gallery mode) of the mentioned dielectric sphere. As the following figure shows, an optical fibre is used to transfer light from a tuneable laser into the sphere. For this purpose, the part of the optical fibre which is in contact with the dielectric sphere is stripped to about 10μm diameter. The intensity of transmitted light after going through the microsphere is detected by a photodiode.
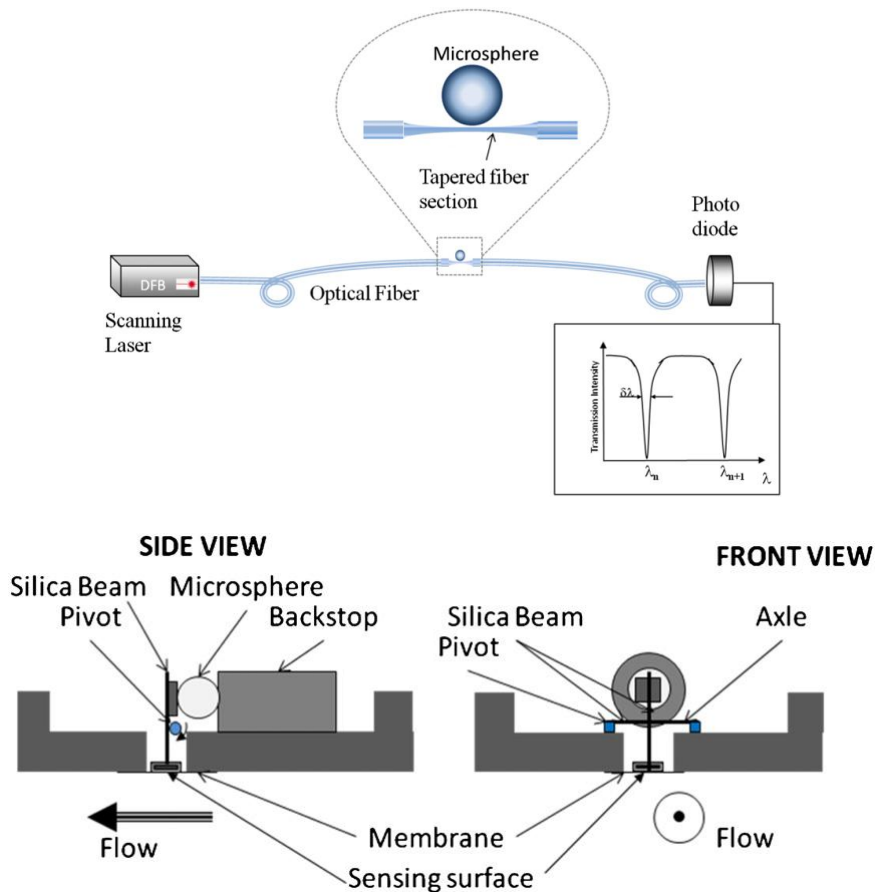
Figure 2-5- Schematic figure of the side view and front view of the WGM optical sensor [13].

The mechanical concept of this optical sensor is similar to the floating element in which shear stress is detected by floating element movement. The advantage of WGM is that it responds to displacements of the order of nanometers to measure the force imposed by the flow.

The sensor can be used in a large range of Reynolds numbers. Sphere material and size affects the sensor resolution when it is applied in different types of flows. Resolution will be increased by softer sphere material; however, the frequency reduction should be taken into account. Thus, a trade off between the resolution and bandwidth is required.

2.2.4. Electrochemical probes

One well-known indirect measurement method is based on electrochemical sensors. WSS measurement using a flush-mounted electrochemical probe was reported by J.E. Mitchell and T.J. Hanratty (1966) [14]. The principle of operation is based on the mass transfer from the probe to the fluid depending on the shear rate at the wall. A rectangular, electrically conducting strip is flush mounted on the wall. The concentration of a chosen chemical species produced at the surface of the film by electrochemical reduction, is maintained constant on this film –to do so, a current is required to counter the variation in rate of mass transfer due to the WSS fluctuation. This current variation may be calibrated to obtain WSS variation. Mitchell and Hanratty (1966) [14] used the following electrochemical reaction:

$$Fe(CN)_6^{-3} + e^- \rightarrow Fe(CN)_6^{-4}$$
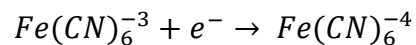
The rate of mass transfer can be obtained from the measured current with Faraday's law [15]. The long side of the sensor is perpendicular to the flow direction to make the

sensor insensitive to spanwise fluctuations. There are some limitations on the physical size of the sensor to keep the concentration boundary layer within the viscous sublayer, in which transfer by molecular viscosity dominates momentum transfer by turbulent velocity fluctuations.

The mass balance equation used for two-dimensional fluid field is:

$$\frac{\partial C}{\partial t} + u\frac{\partial C}{\partial x} + v\frac{\partial C}{\partial y} = D\left(\frac{\partial^2 C}{\partial x^2} + \frac{\partial^2 C}{\partial y^2} + \frac{\partial^2 C}{\partial z^2}\right), \qquad \textbf{Eq. 2-4}$$

where, C is defined as concentration, u and v are velocities in streamwise and normal directions, D is mass diffusivity, and x, y and z are streamwise, spanwise and normal directions, respectively. Some assumptions were made by Mitchell and Hanratty to simplify the problem; the flow is considered as a homogeneous flow; the sensor size is selected so that the concentration boundary layer is within the viscous sublayer. Hence we may replace velocity u by sy, where s is the shear rate associated with the velocity profile $u(y)$ in the sublayer, assumed to be linear for instantaneous profiles. Natural convection, as well as diffusion in the streamwise direction are assumed negligible compared to forced convection. If streamwise thickness of the concentration boundary layer is small compared to spanwise thickness, the spanwise diffusion term may be dropped. Using all these assumptions as well as a quasi-steady state assumption yields the following equation:

$$sy\frac{\partial C}{\partial x} = D\frac{\partial^2 C}{\partial y^2} \qquad \textbf{Eq. 2-5}$$

In this circumstance, the magnitude of the mass transfer rate N can be shown to be related to the shear stress τ by $\sim \tau^{1/3}$, Leveque (1928) [16].

The assumptions made in this method put some restrictions on the design and application of electrochemical sensors, since the thickness of the concentration boundary layer should be less than the viscous sublayer, $\delta_{c}/\delta_{v} < 1$. For this condition to be true, Mitchell and Hanratty showed the following limitation is needed:

$$L^+ < 64 \, Sc,$$

where Schmidt number Sc=ν/D.

Application of this probe in turbulent flows gives electrical responses which are simply related to the shear stress. Stronger fluctuations tend to change the concentration more strongly in the probe. The main advantages of this probe are that the flush mounted probes do not interfere with the flow, and the mass transfer only occurs between the sensor and fluid. The errors caused by transport through the substrate, which are unavoidable in conventional thermal sensors, as we shall see, are not significant. The use of the advection-diffusion equation (Equation 2-4), gives it a very similar theoretical basis as the thermal sensor, and in some ways represents an ideal to which thermal sensing can aspire to. However, the special solution chemistries requirements for measurement restrict the electrochemical probe to limited laboratory use –we cannot extend its use at all to measurements in air, for example.

2.2.5. Near wall hot wire

Measuring the mean and fluctuating wall shear stress in turbulent flow can be done by a thermal resistive hot wire mounted at a small distance (only a few wire diameters) from the wall. The sensitivity of the sensor is related to the distance from the wall, as the velocities very close to the wall are small at low Re numbers. Sensitivity can be increased by increasing distance from the wall, but a necessary restriction is that the wire be mounted within the viscous sublayer. In this type of probe, as in the other thermal wall shear stress sensors, heat conduction to the wall can cause large errors; the velocity measured by the hot wire would not be exactly the local velocity, due to intrusion by the probe. Heat transfer to the wall changes the value of measured shear stress by the hot wire from the true shear stress. Wagner (1991) derived the relationship between these two values [17]:

$$\tau_m = \tau_w - 0.55 \sqrt{\frac{\rho^2 \vartheta}{h^2} \tau_w + 3.2 \frac{\rho^2 \vartheta}{h^2}}$$

Eq. 2-6

τ_m and τ_w are the measured value and the true value of the wall shear stress. h shows the distance at which the hot wire is located from the wall. Sturzebecher *et al.* (2001) made a cavity (0.075-0.1 mm) beneath the flush-mounted hot wire (R=2.5 µm) to reduce the effect of the substrate. They could also increase signal-to-noise ratio by operating the system at a higher overheat temperature without thermal damage to the system [18]. They have used a single sensor and an array of their sensors in a laminar boundary layer in a wind tunnel and in flight experiments on a glider wing.

2.2.6. Thermal sensing using flush-mounted WSS sensors

A very similar type of electrochemical probe is a thermal shear stress sensor using a hot film flush-mounted with the wall. The amount of heat transfer is considered in this case, instead of mass transfer, as the quantity showing the fluctuation strength of WSS. The operating principle of thermal sensors is based on transformation of WSS, through heat transfer rate, to voltage. A thin heated sensing element is flush mounted on a surface exposed to the flow.
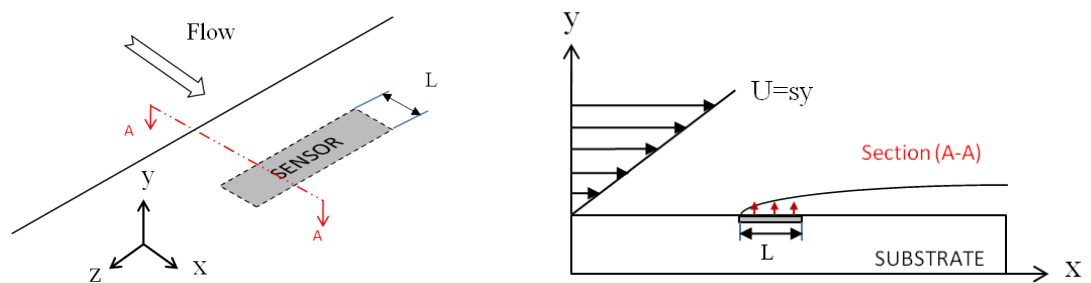
Figure 2-6- Schematic figure of a single-element thermal WSS sensor. x, y, and z represents streamwise, wall normal and spanwise directions, respectively.

The sensor is heated to maintain it at a fixed chosen temperature above the fluid, during operation. The cooling rate of the sensor depends on the strength of the WSS fluctuation. The fluctuating current required for generating heat in the sensor to maintain it at a constant temperature is measured through the voltage drop across its resistance using an AC Wheatstone bridge circuit with a fast servo-amplifier for feedback.
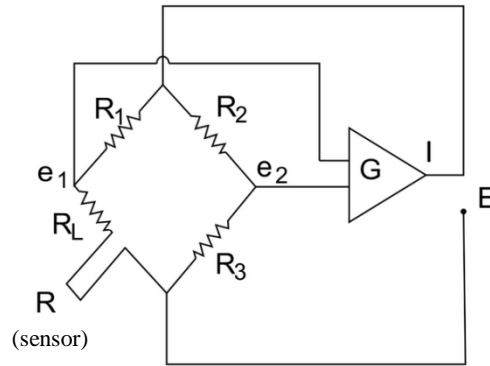
Figure 2-7- An AC wheatstone bridge circuit with a fast feedback servo–amplifier adjusts the current *I* and heat generated $(I^2 R)$ in the probe, to offset cooling by the flow, and maintains the probe at a constant temperature.

Thus, the measured voltage required to keep the sensor at a constant temperature yields the measurement of the wall shear stress. The following calibration equation is used for the voltage and shear stress relationship.

$$E^2 = A\tau^{1/3} + B$$

<div align="right">**Eq. 2-7**</div>

E and τ denote the voltage and shear stress, respectively. Constants A and B are dependent on the measurement condition. More details about this relation are provided in Chapter 3.

Using a material with higher temperature coefficient of resistance (TCR) for the hot film enables faster time response. Recent microfabrication techniques have been able to reduce the thermal sensor size with the hope of improving spatial resolution. Initially, there was hope that the non-intrusive behavior of this type of sensor as well as its high temporal resolution, would make it applicable in many situations. However, the heat conduction to the substrate from a single-element hot-film sensor, regardless of its size, introduces significant limitations. Such a sensor could operate with calibration as given by Eq 2-7 only if it is located on a perfect thermal insulator as substrate.

The nature of the sensor response depends appreciably on the temperature distribution associated with the strong rate of conduction into the substrate, dependent on the ratio of thermal conductivities of the fluid and the solid substrate. This is made clear in the review of Alfredsson *et al*. (1988) [19], which notes that experiments in low conductivity fluids such as oil and air show pronounced errors, while measurements in water fare better. They have tabulated the streamwise WSS fluctuation intensity (the mean-normalized rms value, $\acute{\tau}_x/\tau$) from experiments with several fluids. For water, the values range from 32-40% [19]. The values of $\acute{\tau}_x/\tau$ for air in two different flow types, channel and turbulent boundary layer, reported by Chambers (1982) *et al.* [20], and Thomas (1977) [19] are 0.06, and 0.12, respectively. Suzuki and Kassagi (1992) also reported a 20% underestimation in streamwise velocity intensity when a single probe with almost 35 viscous unit lengths is used near the wall [21]. As we shall see, these small rates of $\acute{\tau}_x/\tau$ reported when air is the flow medium may be explained by a low value of the ratio of thermal conductivities of the fluid to that of the solid.

By heat diffusion into the substrate, the given energy to the sensor would not be released directly to the fluid and would cause some errors such as spatial averaging, phase shift, and amplitude attenuation (these errors will be more discussed in Chapter 3). Heat penetrating the substrate from the hot film eventually reaches the fluid from the interface. The part of heat that warms the upstream, in addition to weakening direct heat transfer from the sensor to the fluid causes a temperature change ahead of the sensor. This would lead to a serious problem in dynamic measurements, as the flow characteristics may vary considerably by the time it reaches the sensor. More significantly, the effective solid surface area through which solid-to-fluid heat transfer

occurs can be much larger than the physical sensor length. One can claim to make a very small thermal sensor using microfabrication techniques to measure small fluctuations, yet this claim is not acceptable, as the effective size of the sensor is significantly bigger than the physical size. Additionally, as we shall see, the preheated length is changed dramatically with different fluctuations or velocities, and the equivalent sensor length extends or shrinks depending on the given shear stress strength.

The advantages and limitations of each sensor named so far have been presented in following table for a fair way of comparison:

Table 2-1- Summary of advantages and disadvantages of various WSS sensors

Sensor	Advantages	Disadvantages
Floating element	• Direct method	• The flow running under the element into gaps • Trade off for the design of geometry and mechanical properties of the sensor elements is required • Response can be sensitive to pressure
Optical probe	• Only displacements in the order of nanometer are required to measure shear stress • The sensor can be used in a large range of Reynolds numbers	• Trade off between the resolution and bandwidth imposes constraints
Electrochemi-cal probes	• The probe does not interfere with the flow • The probe does not suffer from transport to the substrate	• Special solution chemistries are needed • Restricted to laboratory use, no usage in air
Near wall hot wire	• used to measure flow parameters very close to wall	• Errors due to heat conduction to the substrate • Trade off between sensor sensitivity and the distance from the wall is required
Thermal WSS sensors	• Non-intrusive method • Applicable in a broad range of applications • High temporal and spatial resolution	• Heat conduction to the substrate
Micro pillar	• Detecting two dimensional WSS distribution • High temporal and spatial resolution	• Pillar height can exceed viscous sublayer, especially at high Re numbers • High influence of cylindrical aspect ratio on deflection, high value of $\frac{L_P}{D_P}$ is needed • Spatial averaging error caused by long micro-pillar • Trade off between flexibility as well as mechanical properties of the sensor and fluctuations strength is required • Tip bending detection by an optical system

2.2.7. Available methods to overcome thermal WSS sensors limitations

Several solutions have been examined to remove or modify the limitations associated with conventional sensors. Aoyagi *et al*. (1986) developed a sensor made of two commercial probes of 0.1mm×0.9mm nickel films. One probe operated as the sensor from which the measured data are taken. The other one is located right beneath the main probe to block the heat dissipation into the substrate [22]. They showed that both the sensor and guard heater should be kept at the same temperature in order to minimize the static calibration curve dependency on the wall temperature.

Another method uses a vacuum or air pocket underneath the hot film. Q. Lin *et al*. (2004) studied MEMS thermal shear stress sensors including a hot film placed on a silicon nitride or Parylene diaphragm [23]. An air/vacuum pocket beneath the diaphragm separates the sensor from the substrate. The diaphragm is flush-mounted with the wall and the heating element is perpendicular to the flow direction. By this means, they reduced the influence of substrate on fluid temperature before and after the sensing element. The measuring process is similar to that of the constant temperature thermal probe. The schematic figure of the sensor is shown in the following figure:
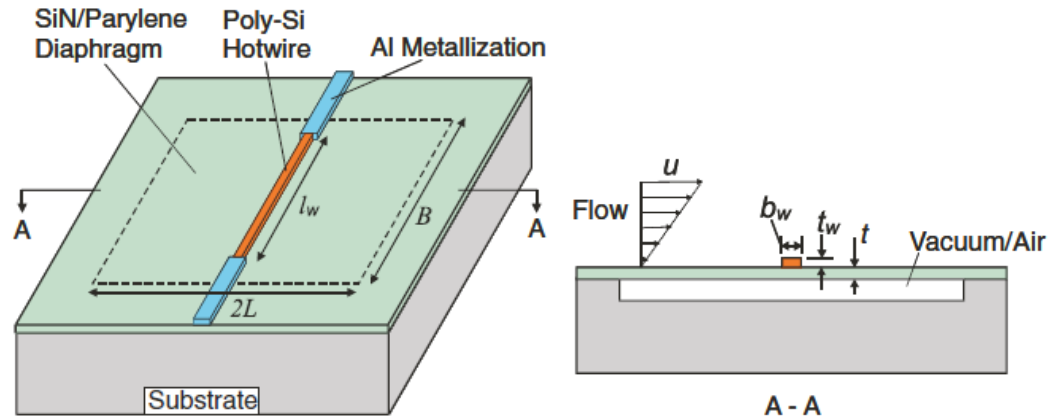
Figure 2-8- Schematic figure of a thermal shear stress probe including an air/vacuum pocket [23].

Several sensors of various sizes have been made by this group; as an example, one of the MEMS sensors is made of a 210×210×1.5 (μm^3) diaphragm where 1.5μm is the thickness of the membrane and the two other numbers represent the length and width. The length of the heating element perpendicular to the flow direction is 150μm; its streamwise and normal dimensions are 3μm and 0.5μm, respectively.
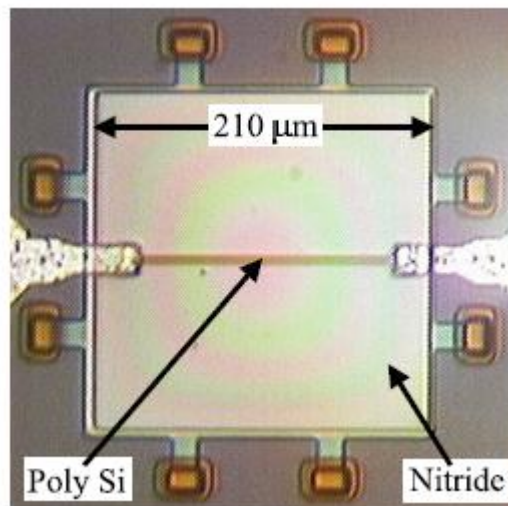
Figure 2-9- MEMS shear stress sensor made by Q. Lin et al., The diaphragm is made of nitride [23].

The sensors were tested in a wind tunnel; they have observed the experimental data from their MEMS probes was incongruous with the classical theory used for conventional thermal sensors ($q \sim \tau^{1/3}$). They proved the lack of a thin thermal boundary layer at the MEMS sensor leads to experimental and theoretical variation.

Yamagami *et al*. also developed a prototype feedback control system including hot film MEMS sensors on air cavity and actuators. 18 wall shear stress sensors are placed in spanwise direction. The thermal sensors with backside contact are shown in following figure.
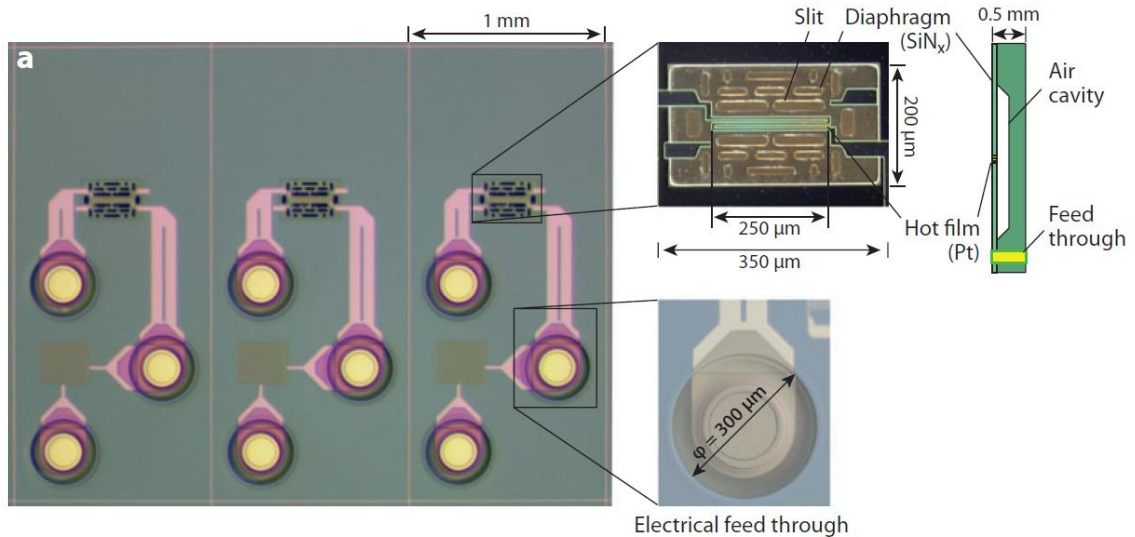
Figure 2-10- Hot film wall hear stress sensors made by Yamagami [24].

Hot film material is made of platinum deposited on a SiN_x diaphragm of 1μm thickness and ($400 \times 250 \mu m^2$) width. Beneath the sensor there is a cavity to reduce heat diffusion to the substrate. Required current for the sensor is fed through the backside of the chip from a flexible print circuit board.

Some concerns in using a diaphragm to suspend the sensor from the substrate are the conductivity and very small thermal capacity of the membrane. Even though the substrate is separated in this case, the thermal conductivity of the diaphragm spreads the heat generated in the sensor into a large area. This means the measurement is done through a larger area than the small sensor. Thus, the spatial averaging error would not be negligible, since heat transfer to the fluid is happening from the sensor and membrane. The low thermal capacity of the membrane changes the equivalent length of the sensor rapidly depending on the current fluctuation, since the heat can be picked up or spread rapidly in the diaphragm. Strong fluctuations can pick up more heat from the upstream side; whereas, the small fluctuations lead to bigger preheated area. Consequently, in turbulent flows, there may not be enough time for complete heat transfer between the solid parts and the fluid, in that the response from the device may also include the information about the previous fluctuation.

Another approach suggested by R. Bhiladvala (2009) is using a guard heater – controlled by separate anemometer circuit– around the sensor with the same temperature; by this means, the temperature gradient at the edge of the sensor is forced to be zero [25]. Thus, the heat transferred from the sensor to the surroundings at the same plate will be blocked. The main advantage of this design is that the sensor length in which heat transfer to fluid happens would be marginally different from the physical length of the sensor. We can eliminate the errors caused by spatial averaging to some degree by making a sensor as small as the noise to signal ratio allows.

A study of the heat transfer process is needed in order to find a solution to overcome the deficiencies of conventional thermal single–element sensors.

3. Theory, methods and design

3.1. Theoretical considerations

To analyze the thermal WSS sensor response in different conditions, here we investigate the heat exchange between the substrate and fluid, with convection of heat depending on the shear stress, and diffusion of heat in the solid domain. Signals from single-element thermal WSS sensors include some errors due to heat conduction in the substrate –which is termed indirect heat transfer. The total generated heat (Q_t) in the probe is divided into two main direct (Q_d) and indirect (Q_I) heat transfers.

Fluid

Q_{Iu} Q_d Q_{Id}

Substrate Q_I
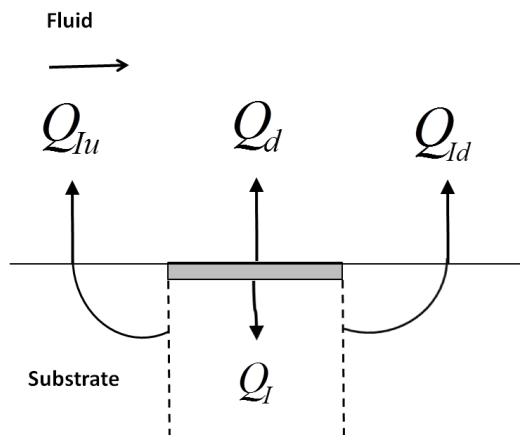
Figure 3-1- Heat released from single-element sensor to the surroundings, Q_d: direct heat transfer, Q_I: indirect heat transfer, Q_{Iu}: upstream indirect heat transfer, Q_{Id}: downstream indirect heat transfer

$$Q_t = Q_I + Q_d$$

Eq. 3-1

As we shall see later in this chapter, Q_I contributes significantly to two errors - spectral distortion and variable spatial averaging with fluctuation strength.

According to available literature, the relationship between shear stress and direct heat transfer can be defined by the following equation:

$$\tau_w \sim Q_d^3 \qquad \text{Eq. 3-2}$$

A simple derivation of these parameters has been done by Ling (1963); for more details see Kalumuck [26]. As a fluid with α_f thermal diffusivity passes a hot film, the thermal boundary layer with $\delta_T(x)$ starts to grow at the leading edge of the film as illustrated in Figure 3-2:
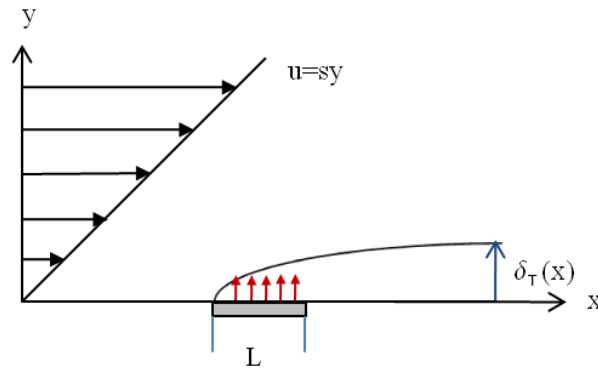
Figure 3-2- Schematic figure of thermal boundary layer and viscous sublayer.

This figure shows the development of thermal boundary layer within the viscous sublayer, where velocity changes linearly with velocity gradient (see section 3.1.1). The time needed for the heat to reach the thermal boundary layer thickness is defined as:

$$t = \frac{\delta_T^2}{\alpha_f} \qquad \text{Eq. 3-3}$$

This time is equal to the time that the fluid passes the distance x:

$$t = \frac{x}{u} = \frac{x}{s_x \delta_T} \qquad \therefore \qquad \frac{x}{s_x \delta_T} \sim \frac{\delta_T^2}{\alpha_f} \qquad \text{Eq. 3-4}$$

$$\delta_T^3 \sim \frac{x\,\alpha_f}{s_x} \qquad \therefore \qquad \delta_T \sim \left(\frac{x\,\alpha_f}{s_x}\right)^{1/3} \qquad\qquad \text{Eq. 3-5}$$

The inverse relation of heat transfer to the thermal boundary layer thickness gives the following relation:

$$q \sim \frac{1}{\delta_T} \sim \left(\frac{s_x}{x\,\alpha_f}\right)^{1/3} \qquad\qquad \text{Eq. 3-6}$$

In order to further understand the system, its limitations, and to be able to improve the probe by modifying the design, we need to solve the governing equations.

3.1.1. Governing equations

To obtain the temperature distribution in the sensor and fluid passing over it, the equations governing heat transfer in the fluid, solid and at the interface between them, are presented in this section.
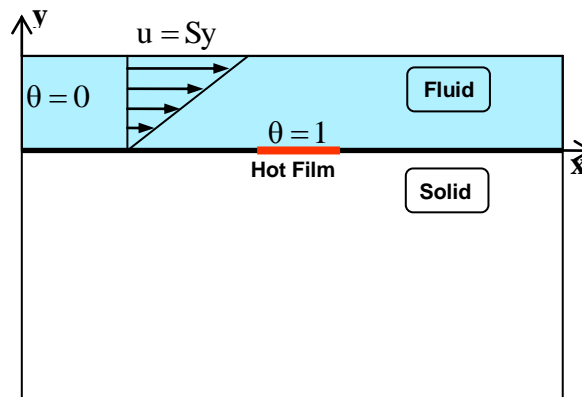
Figure 3-3- Defining sketch for geometry and non-dimensional temperature (θ).

The non-dimensional temperature (θ), with values in the range [0,1] is defined by:

$$\theta = \frac{\left(T - T_f\right)}{\left(T_w - T_f\right)}$$

Eq. 3-7

T_w is the uniform temperature of the wall hot film which is maintained higher than its surroundings; T_f denotes the ambient temperature of fluid that is not affected by the hot film.

Temperature field in the fluid can be described by the energy equation for incompressible, constant property flow:

$$\frac{\partial\theta}{\partial t} + u\frac{\partial\theta}{\partial x} + v\frac{\partial\theta}{\partial y} + w\frac{\partial\theta}{\partial z} = \alpha_f\left(\frac{\partial^2\theta}{\partial x^2} + \frac{\partial^2\theta}{\partial y^2} + \frac{\partial^2\theta}{\partial z^2}\right),$$

Eq. 3-8

where (x,y,z) and (u,v,w) are the co-ordinates and velocity components, in the streamwise, wall-normal and spanwise directions, respectively.

In order to simplify the equations, we apply the common assumptions used for different calculations. First of all, homogeneous flows with negligible viscous dissipation are described by Equation 3-8. We ignore the heat transport by spanwise velocity fluctuation w, in comparison to streamwise fluctuation, u. This assumption is true if the long side of the rectangular-shaped sensor is located perpendicular to the flow direction. By this means, thermal boundary layer thickness due to spanwise flow will be considerably bigger than the thermal boundary layer thickness for streamwise flow. The large thermal capacity of the thick thermal boundary layer in the spanwise direction renders the sensor insensitive in this direction in comparison to the mean flow direction. Fluctuations normal to the wall are also found to be negligible because of the existence of

the solid boundary. Natural convection does not play a significant role compared to forced convection, particularly for strong fluctuations.

If the hot element is small enough in the direction of the mean flow (streamwise), the thermal boundary layer will be within the viscous sublayer in which $\bar{u}$ and $\acute{u}$ vary linearly with y. In this region, mean velocity and fluctuations are given by $\bar{u} = \bar{s}_x y$, and $\acute{u} = \acute{s}_x y$, where $s_x = \bar{s}_x + \acute{s}_x$ is the velocity gradient at the wall. The shear rate has both steady-state and time-dependent terms; it is described by two parameters, s_{x0} and frequency ω:

$$s_x = s_{x0}(1 + a\cos(\omega t))$$

<div align="right">Eq. 3-7</div>

In the study in this thesis, we focus on removing the problems associated with steady-state heat conduction errors. The time dependent term is not explicitly `considered in this research. For notational convenience, s_x will be used to represent the steady-state part of velocity gradient in the following sections.

Shear stress in streamwise direction is $\tau_w = s_x \mu$, where μ is the dynamic viscosity of the fluid.

Using these assumptions, the Equation 3-8, after the substitutions, reduces to:

$$\frac{\partial \theta}{\partial t} + s_x y \frac{\partial \theta}{\partial x} = \alpha_f \left(\frac{\partial^2 \theta}{\partial x^2} + \frac{\partial^2 \theta}{\partial y^2} + \frac{\partial^2 \theta}{\partial z^2} \right)$$

<div align="right">Eq. 3-8</div>

The temperature distribution in the solid substrate is calculated by the energy equation for the substrate. With α_s as the solid's thermal diffusivity, the equation is:

$$\frac{\partial \theta}{\partial t} = \alpha_s \left(\frac{\partial^2 \theta}{\partial x^2} + \frac{\partial^2 \theta}{\partial y^2} + \frac{\partial^2 \theta}{\partial z^2} \right)$$

<div align="right">Eq. 3-9</div>

At the interface between wall and fluid the boundary condition is:

$$k_s \left(\frac{\partial \theta}{\partial y} \right)_s = k_f \left(\frac{\partial \theta}{\partial y} \right)_f$$

<div align="right">Eq. 3-10</div>

Where k_f and k_s are the thermal conductivities of the fluid and solid, respectively. To better understand the significance of parameters, non-dimensionalised form of governing equations were derived, which will be discussed in the following section.

3.1.2. Non-dimensional equations and parameters

The energy equations used for the solid, fluid, and interface are further simplified by the dimensionless form. Replacing $t, x, y,$ and z by dimensionless parameters t^*, x^*, y^* and z^*, in both fluid and solid, changes the governing equations to the non-dimensional form.

$$t^* = t. \omega \quad , \quad x^* = \frac{x}{L} \quad , \quad z^* = \frac{z}{W}$$

<div align="right">Eq. 3-11</div>

Where, ω is the frequency of the applied shear at any instant, L is the hot film length at mean flow direction, and W is the length of the hot film perpendicular to the mean flow. The thermal boundary layer thickness (δ) and hot film length (L) are used to non-dimentionalise the wall normal coordinate y in fluid and solid area, respectively. Correspondingly, $y^* = \frac{y}{L}$ is replaced in the solid energy equation and $y^* = \frac{y}{\delta}$ in the fluid. By substituting the dimensionless parameters in the governing equations, a simpler form of the energy equations is obtained. For notational convenience, as frequently used, we

drop the star in the non-dimensionalized equations. Therefore, the symbols $x, y, z,$ and t and derivatives of temperature θ with respect to these variables, represent dimensionless quantities of order 1, in the equations below.

The modified governing equations for the fluid, solid and interface are written as follow, in order, as:

$$\omega^* \left(\frac{\delta^2}{L^2}\right) \frac{\partial \theta}{\partial t} + Pe \left(\frac{\delta}{L}\right)^3 y \frac{\partial \theta}{\partial x}$$

$$= \frac{\partial^2 \theta}{\partial x^2} \left(\frac{\delta^2}{L^2}\right) + \frac{\partial^2 \theta}{\partial y^2} + \frac{\partial^2 \theta}{\partial z^2} \left(\frac{\delta^2}{L^2}\right) \left(\frac{L^2}{W^2}\right) \qquad \text{Eq. 3-12}$$

$$\omega^* \left(\frac{\alpha_f}{\alpha_s}\right) \frac{\partial \theta}{\partial t} = \frac{\partial^2 \theta}{\partial x^2} + \frac{\partial^2 \theta}{\partial y^2} + \frac{\partial^2 \theta}{\partial z^2} \left(\frac{L^2}{W^2}\right) \qquad \text{Eq. 3-13}$$

$$\frac{K_s}{K_f} \left(\frac{\delta}{L}\right) \left(\frac{\partial \theta}{\partial y}\right)_s = \left(\frac{\partial \theta}{\partial y}\right)_f \qquad \text{Eq. 3-14}$$

Some independent dimensionless parameters can be defined for the above equations. The Pe number is associated with the velocity gradient, sensor streamwise length and the fluid thermal diffusivity. If the velocity is replaced by $s_x L$, a new form of the Peclet number will be obtained.

$$Pe = \frac{s_x L^2}{\alpha_f} \qquad \text{Eq. 3-15}$$

The non-dimensional frequency in time-dependent terms can be written as:

$$\omega^* = \frac{\omega L^2}{\alpha_f}$$

<div align="right">**Eq. 3-16**</div>

Some other ratios such as: ratio of sensor physical lengths in streamwise and spanwise (L/W), thermal boundary layer and streamwise sensor length (δ/L), solid and fluid thermal conductivities (k_s/k_f), and fluid-substrate thermal diffusivities (α_f/α_s) should be taken into account for the sensor performance. The last term is important when the time required for the heat to release into the fluid via the substrate is comparable with the time for direct hot film-fluid heat transfer. The chosen material for the substrate plays a crucial role especially for fluids with low thermal conductivity. The non-dimensional relationship between shear stress and heat convection is defined by the Leveque solution.

3.1.3. Leveque solution

The two dimensional steady-state heat transfer problem has been solved by Leveque (1928) for a simpler geometry. The solution provides a simple algebraic relation between shear stress and heat transfer rate [16].

As we mentioned, the shear stress magnitude is related to the amount of heat transfer from the sensor ($Q \sim \tau$). Leveque proved that heat flux is related to one-third the power of shear stress, as indicated in the following relation:

$$\text{Nu} = 0.807 \, \text{Pe}^{1/3}$$

<div align="right">**Eq. 3-17**</div>

This algebraic relation is derived assuming all the parameters except streamwise convection and normal diffusion in the fluid are kept at zero, and that there is no heat conduction in the substrate (perfect insulator). More details about the Leveque solution can be found in Appendix A.

The measured WSS values obtained by using this simplified algebraic relation for calibration would indeed be reliable if the terms assumed to be zero in this Leveque solution are rendered negligible by design; otherwise, the Leveque solution as calibration scheme needs to be corrected. However, these assumptions are not appropriate in reality with conventional single-element sensors, which suffer from several errors including substrate conduction, streamwise and spanwise heat conduction in the fluid, and attenuation due to thermal boundary layer capacitance in the fluid. Among all the errors, substrate conduction has the strongest influence on the sensor performance. How the thermal conductivity of the substrate causes strong deviations from the analytical algebraic relation is presented in the following section.

3.1.4. Power dissipation in the sensor and shear stress relation

As mentioned earlier, probe calibration curves are commonly expressed by two non-dimensionalized parameters: the Nu number for non-dimensionalized heat transfer and the Pe number for representing non-dimensional shear stress. By substituting hL/k, in place of the Nusselt number Nu number and $s_x L^2/\alpha_f$, in place of the Peclet number Pe the Leveque relation can also be written as:

$$\frac{q}{\Delta T} = 0.807 \; \frac{C_P^{1/3} k_T^{2/3}}{L^{1/3}\mu^{1/3}} (\rho\tau_w)^{1/3}$$

Eq. 3-18

This relation shows the influence of fluid and sensor parameters on the amount of heat transfer. The rate of heat transfer q is related to electric current I and sensor film electrical resistance R, which define the probe power consumption:

$$q = I^2 R$$

<div align="right">**Eq. 3-19**</div>

Therefore, the variation of heat transfer can be read by electrical current fluctuation, since the temperature of the heating element is maintained constant by rapid current change from the fast amplifier of the controlling AC Wheatstone bridge circuit. The last two equations can be used to associate the local shear stress and sensor power consumption if the Leveque assumptions are applied. However in reality, electric current and shear stress relation is derived by the following equation:

$$\frac{I^2 R}{\Delta T} = A(\tau_w)^{1/3} + B$$

<div align="right">**Eq. 3-20**</div>

Values of constants A and B are 0.807 and zero in the Leveque equation. Constant B represents the amount of heat released into the substrate and natural convection. These two terms need to be found experimentally. Kalumuck (1983) provided a schematic representation of the calibration curve as shown in the following figure [26]:
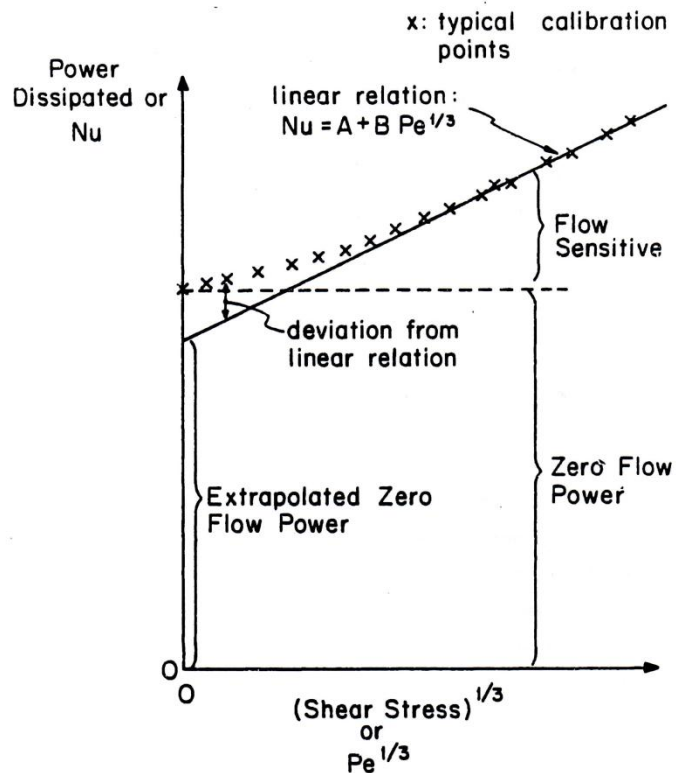
Figure 3-4- Sketch of power dissipation and shear stress relationship from Kalumuck [26].

The slope of this line indicates the sensitivity of heat transfer to the shear stress. The value obtained by extrapolation of the line at zero shear stress represents the amount of heat dissipation from the heating element into the fluid due to natural convection. As we will see, the significant rate of heat loss to the substrate for small shear values complicates the measuring process and introduces some limitations on WSS thermal sensors.

3.2. Limitations of Thermal single-element WSS sensors

Some of the physical processes which happen in reality and are not considered in analytical solution can be listed as: variable spatial resolution, spatial averaging, heat diffusion to the substrate, substrate-to-fluid heat conduction through the interface, streamwise and spanwise heat conduction to the fluid, resulting in spurious amplification of the low frequency end of the spectrum, spectral attenuation due to the fluid thermal boundary layer, and phase distortion. The following figure shows the distortion in measured signals. In an ideal case, there is no time lag between the imposed shear stress and change in the voltage in the sensor.
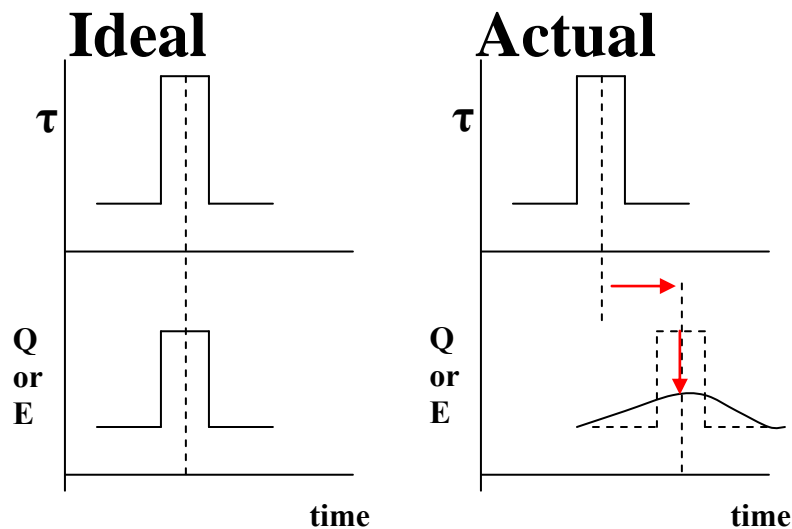
Figure 3-5- Schematic figure of response distortion received by a thermal WSS sensor.

The value of each point on the voltage diagram is related to one-third the power of shear stress at the time of interest. However, in the actual case, the voltage-shear stress relationship cannot be simply defined. In addition, time lag distortion puts some

limitations on sensor application such as finding the correlation between the wall shear stress and the velocity at a distance from the wall.

Some of the limitations are explained in more details in following sections. For this purpose, the non-dimensional energy equations are concerned. One fact derived from the dimensionless fluid energy equation is the dependencies of (δ/L) to Pe in order to keep $Pe \left(\frac{\delta}{L}\right)^3$ of order one.

3.2.1. Frequency response

To measure fluctuations in turbulent flows, the thermal boundary layer is often a concern, since it has a noticeable effect on the frequency response. The sensor response in an unsteady situation is highly dependent on the thermal inertia of the boundary layer, which can affect the signals by phase distortion or amplitude attenuation. In order to detect the sensor behavior in a dynamic flow, it should be noted the unsteady term in the fluid energy equation implies that frequency should be $\sim Pe^{2/3}$ to force this term to be an order of one.

For high frequencies, $\omega^* \gg Pe^{2/3}$, there is not enough time for fast fluctuations to pick up heat from the sensor because of the thermal inertia of the boundary layer. As a result, the sensor does not show any signal after a certain Pe number. This region is truncated and no correction factor can be applied to modify the signals. Subsequently, the pseudo-steady state assumption, which is commonly used to compute the shear stress from measured voltage at any instance by $E^2 = A\tau^{1/3}$, would not be correct.

For small frequencies, $\omega^* \ll Pe^{2/3}$, the sensor is able to respond to the frequency, and the time-dependent term in the energy equation in the fluid can be neglected. In this case, the sensor response is reliable under the condition that the substrate has no conductivity; however, this is hardly possible in reality. Consequently, there is another type of error caused by solid conductivity; the time required for heat to diffuse over length L in the substrate (L^2/α_s) is comparable to $\omega^{*-1}(\frac{\alpha_s}{\alpha_f})$. A greater fraction of heat released by the sensor goes to fluid via the solid and is interpreted as low frequency fluctuations that do not exist. Recall that, in the analytical relation, we assumed the strength of the sensor response is only associated with the amount of heat transferred by hot film to the fluid, not the substrate.

In brief, comparison between the real turbulent spectrum and the one obtained by the analytical method shows a spurious amplification for small ω and an attenuation or complete truncation for large ω. No correction factor can be used for complete truncation, since the sensor does not record any response which can be corrected.
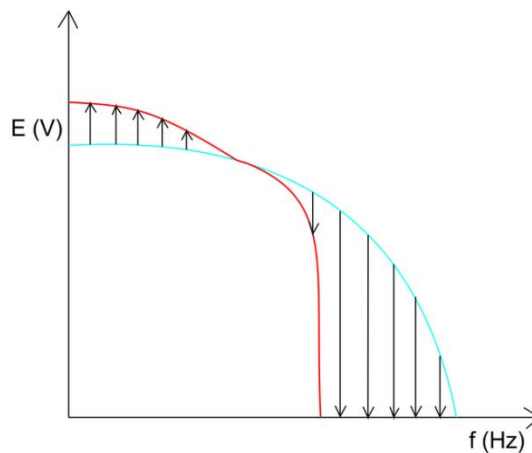
Figure 3-6- Schematic figure of analytical and real frequency response; the blue and red lines indicate analytical and real response, respectively.

As this figure shows, the main part of the signals is distorted due to thermal inertia of the thermal boundary layer as well as the substrate conduction. R. Bhiladvala (2009) presents results showing that only a very small fraction of the spectrum is free from distortion at any range of Reynolds numbers [25].
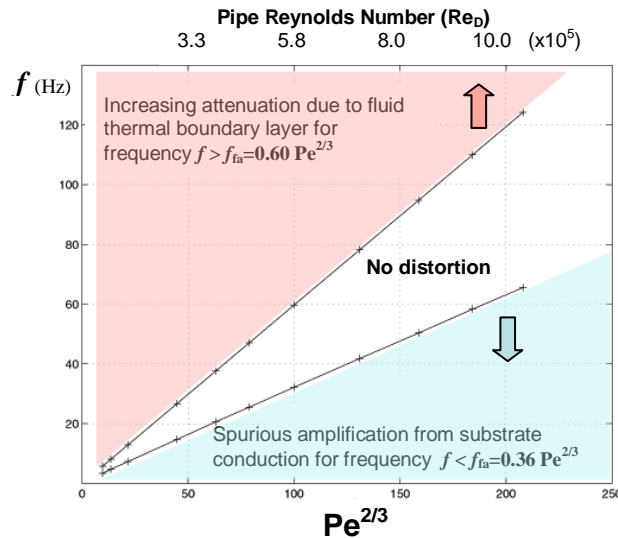
Figure 3-7- Frequency of spectral distortion measured in pipe flow by a single-element sensor [25].

According to this figure, at $Re = 5.8 \times 10^5$ while signals suffer from attenuation at frequencies higher than 60 Hz due to thermal boundary layer inertia, substrate conduction also causes a spurious amplification error for signals with frequencies less than 30 Hz.

3.2.2. Heat conduction through substrate to fluid

As we noted earlier, the heat transfer-fluid shear relation cannot be calculated analytically, since the presence of the thermally conducting substrate changes the amount of heat transfer. Thus, probe performance is not only dependent on the streamwise conduction and normal diffusion in the fluid, but depends also on three-dimensional

conduction in the substrate. The sensor size also affects the amount of heat diffusion in the solid substrate. The dimensionless energy equation for the solid at a steady-state condition indicates the spanwise diffusion in the solid varies significantly with the probe aspect ratio (L/W). Also, choosing (L/W) $<< 1$ reduces the spanwise conduction in the fluid.

In addition, the effect of preheating in thermal WSS sensors should be taken into account; it does not only diminish the amount of direct heat transfer. The main issue in single-element sensors is that the heat required to warm the upstream fluid is provided by the current sent to the sensor. Thus the measured data is not reliable in single-element sensors, as it includes direct, upstream and downstream heating. In other words, we are measuring the average of all fluctuations along the whole area where heat exchange between fluid and solid occurs. The question that arises here is if we can calculate the part of generated heat in the sensor needed for pre-heating and post-heating. If so, we are able to deduct the undesirable heat loss from the received signals. The difficulty is that the pre-heating rate can differ considerably during a measurement of a given Reynolds number, since it varies depending on the present fluctuation.

3.2.3. Spatial averaging

A considerable error in shear stress measurement is due to spatial averaging. This happens when the sensor length is larger than the length scale of the given fluctuation; the response obtained by the sensor shows the average fluctuation strength over the sensor. For the fluctuations of opposite sign over different parts of the heat exchange

area, the sensor may not show any changes in response at all, wrongly indicating that there is no fluctuation. This is an example of loss of resolution due to spatial averaging.

The following figures indicate the spatial averaging error for conventional single-element sensors. These figures show a significant dependency of the actual sensor size to the current fluctuations.
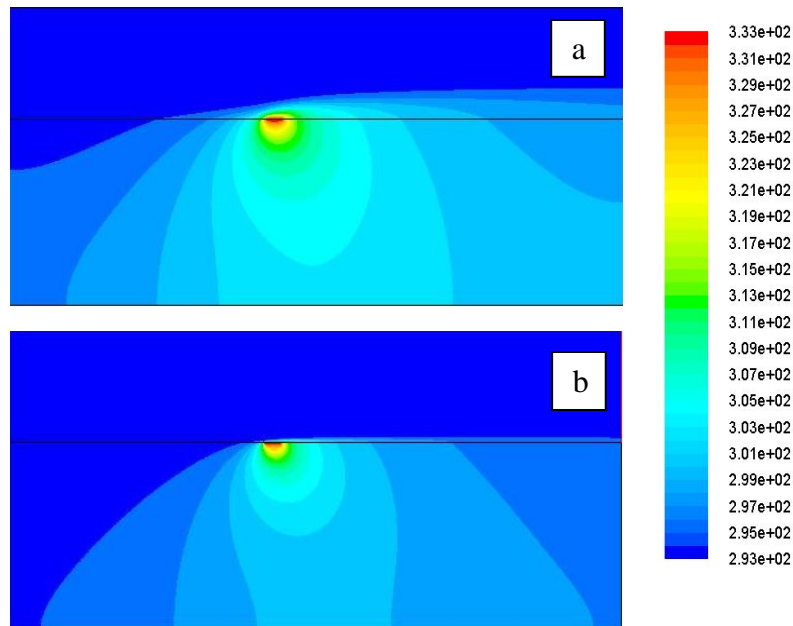
Figure 3-8- Temperature field at a) Pe=30 and b) Pe=3000.

As the figures illustrate, the heat exchange area can be significantly larger than the sensor physical size. This area increases significantly as the Peclet number Pe decreases. In this research, we are focusing on the errors due to substrate conductivity, as it imposes strong distortions in sensor responses in comparison to other errors. In order to remove some of them, various designs for the sensor have been suggested and fabricated so far. A few of these designs were presented in Chapter 2. The performance of guard-heated sensors in a plane as well as guard-heated sensors on two planes is our interest in this

study. Thus, these probes are studied numerically and compared with single-element sensors.

3.3. Numerical investigation

Numerical investigation is used to quantify the real heat transfer process in thermal wall shear stress beyond the simplified analytical solution of the idealized Leveque problem, which assumes zero substrate conduction. Calculating the amount of heat transfer from the sensor directly to the fluid, and the effect of wall temperature on this value is our main concern. In this section, first, we studied a conjugate heat transfer problem for a single-element sensor.

Even though our primary goal is applying the sensor in turbulent flow, the sensor is modeled in the presence of one constant wall shear stress value at a time, to have better understanding of its performance for various fluctuation strengths. Thus, our solution is not time dependent. A computational model of the solution and boundary conditions for the Leveque solution was also made and compared with the analytical Leveque solution, to help test the grid and domain independence of the numerical calculation. Analysis of new designs of thermal shear stress sensors are presented in Chapter 4. All the simulations used Ansys 12.1 (Fluent), and the results were analysed by MATLAB.

3.3.1. Computational domain

This work presents a computational study of a two-dimensional heat transfer problem. The schematic figure of the fluid, solid and hot film domains including the boundary conditions is illustrated in Figure 3-9.
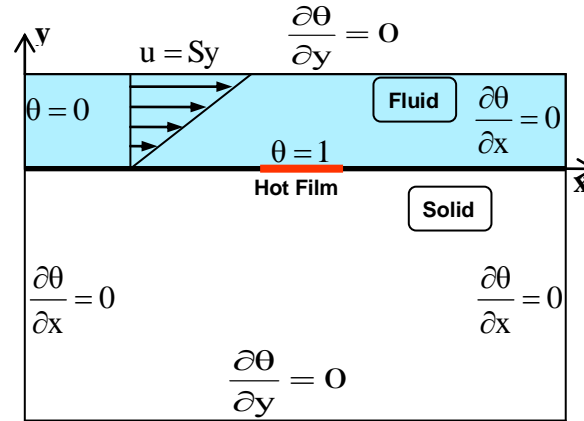
Figure 3-9- Domain and boundary conditions.

As the sensing element should provide a strong feedback for quick response of servo-amplifier current change to shear stress change, nickel, with a high temperature coefficient of resistance (TCR), was chosen for the hot-film sensing element. For the substrate material, silicon dioxide is used, as it has low thermal conductivity.

3.3.2. Boundary conditions

Boundary conditions at three sides of the solid (x, y→∞) are defined as adiabatic:

$$\begin{cases} \dfrac{\partial\theta}{\partial x} \to 0 & ,x \to \pm\infty \\ \dfrac{\partial\theta}{\partial y} \to 0 & ,y \to -\infty \end{cases}$$

In the fluid, $\partial\theta/\partial y \to 0$ far away from the hot film:

$$\frac{\partial\theta}{\partial y} \to 0 \quad ,y \to +\infty$$

Here the symbol for infinity indicates that the boundary locations are chosen far enough from the hot film, so that the solution does not vary with domain size. Fluid enters the system at ambient temperature, cools the hot film, and then leaves the fluid

domain. Thus, the boundary condition at the inlet is defined by $\theta_{inlet}=0$. As the sensor is a hot film with constant temperature, $\theta_{Hot\ film}=1$.

The rate of heat exchange between solid and fluid at the interface is the continuity of heat flux, which we showed, in non-dimensional form, to be:

$$\frac{K_s}{K_f}\left(\frac{\delta}{L}\right)(\frac{\partial \theta}{\partial y})_s = (\frac{\partial \theta}{\partial y})_f$$

Eq. 3-21

3.4. Code validation

To begin with, the accuracy of numerical calculations should be checked. The Leveque problem is the closest problem, for which an analytic solution is known. Grid and domain independence checks for the numerical calculation are thus tested by creating a numerical model closest to the Leveque solution, and comparing numerical results with its analytic solution.

The closest geometry to the analytical model chosen in this study includes only fluid and hot film domains (no substrate), since, for the Leveque problem, the substrate works just as a holder with zero thermal conductivity. An infinite hot film located on a substrate with zero thermal conductivity is considered in the Leveque solution. In order to recreate the same model, we simulated a hot film stretched all the way to the downstream boundary. Figure 3-10 indicates the schematic geometry for the Leveque solution.
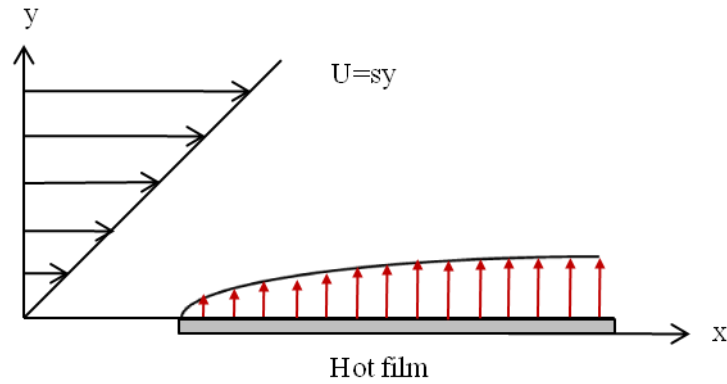
Figure 3-10- Schematic figure of Leveque geometry.

The boundary conditions for the fluid domain for the Leveque validation-model are the same as that of our model the previous model –with the exception of the fluid-solid interface boundary condition. The difference is that the lower wall boundary upstream of the hot-film is defined as an adiabatic wall as the Leveque problem assumes a perfectly insulating substrate. Further, a deviation from the Leveque problem is that axial conduction in the fluid, which cannot be considered negligible at low *Pe* numbers, cannot be forced to be zero as required for the Leveque problem, due to code limitations. Calculated heat transfer from the hot film to the fluid based on the current shear stress is compared with the Nusselt and Peclet number relationship defined by Leveque. Results of this simulation showed a small deviation from the analytical method. Further validation of the code, including fluid and solid domain size influence on the results, as well as grid independency, are shown in following section of this chapter.

3.4.1. Checks for solution independence of mesh density and domain size

A grid independence check was done by comparison of numerical and analytical

solutions for the Leveque problem.
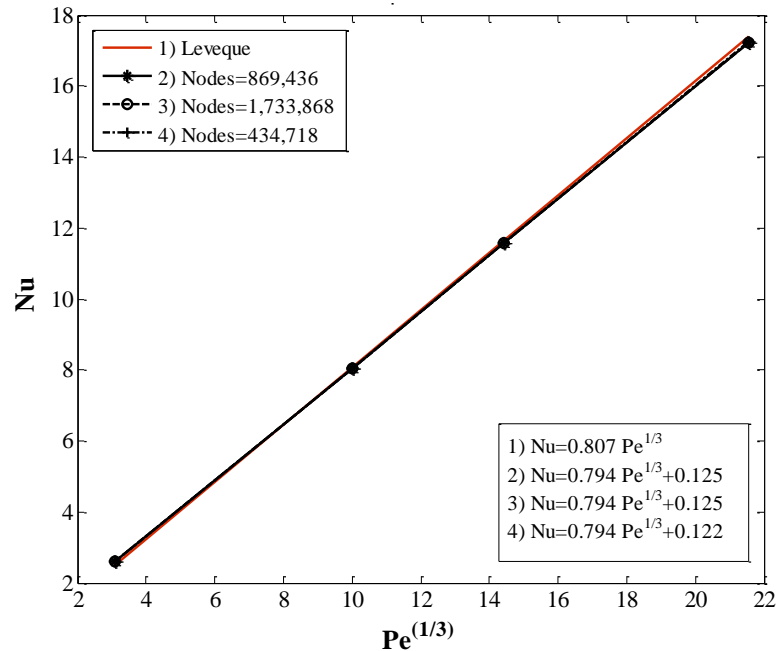
Figure 3-11- Mesh independence check with the available analytical solution.

CFD calculations for three different mesh densities, 0.4, 0.8, and 1.6 nodes per area

$(A \approx 1 \, mm^2)$ are shown. The error of 1.6% of the line slope from the analytic solution is

unchanged if the mesh density is halved or doubled. We are unable to exclude fluid axial

conduction in the numerical calculation with Fluent, but the results here show that the

error from our numerical solution compared to Leveque does not exceed 1.6%.

In the analytical method, the domain is unbounded at right. Note that in the

Leveque solution, the heating element has an infinite length. Since physical restrictions

prevent us from simulating a model similar to Leveque geometry, the boundaries should

be chosen for enough so that their influence on the problem can be ignored.

The heat transfer rate evaluated by the Leveque relation is derived at $\eta = 0$. Since η is defined as $y(S_x/9\alpha x)^{1/3}$ (see appendix A for more details), one of the following conditions needs to be established:

$$\begin{cases} y = 0 \\ \quad or \\ x \to \infty \end{cases}$$

Note that $y = 0$ and length $x \to$ infinity represent the interface, and the streamwise extent of the hot film, respectively. The Leveque solution is valid regardless of the sensor length; at a constant Pe number, if the length of sensor increases, the heat transfer coefficient is lower, such that the Nu number stays at a constant value. We should consider the fact that in the analytical solution, the temperature gradient $\left(\frac{\partial \theta}{\partial x}\right)_{x\to\infty}$ is zero; however, in reality, for this gradient to be negligible, we must ensure that the downstream (exit) boundary is located far enough. Here, we have calculated the Nu values at various downstream distances from the hot film leading edge, to study domain independence.
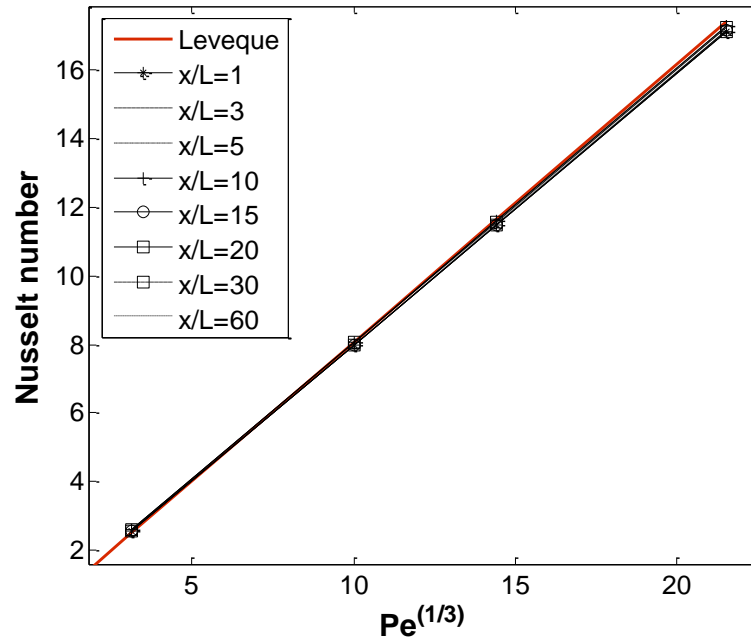
Figure 3-12- Domain independence check with available analytical solution.

L represents the sensor length or the section of the hot film from which heat transfer rate was calculated, and x indicates the distance from hot film leading edge to the end of the domain. We studied several fluid domain sizes for the Leveque solution. In each geometry, heat transfer from some specific lengths of the hot film was calculated; Pe numbers were also chosen based on these lengths.

The slope errors of all listed geometry sizes in comparison to the Leveque solution are less than 2.5%. As we mentioned earlier, this variation includes the numerical errors plus axial conduction in the fluid.

To see how the heat transfer rate changes along the sensor, non-dimensional direct heat transfer from the dimensionless length of the sensor to water for various Pe numbers is indicated in the following figure.
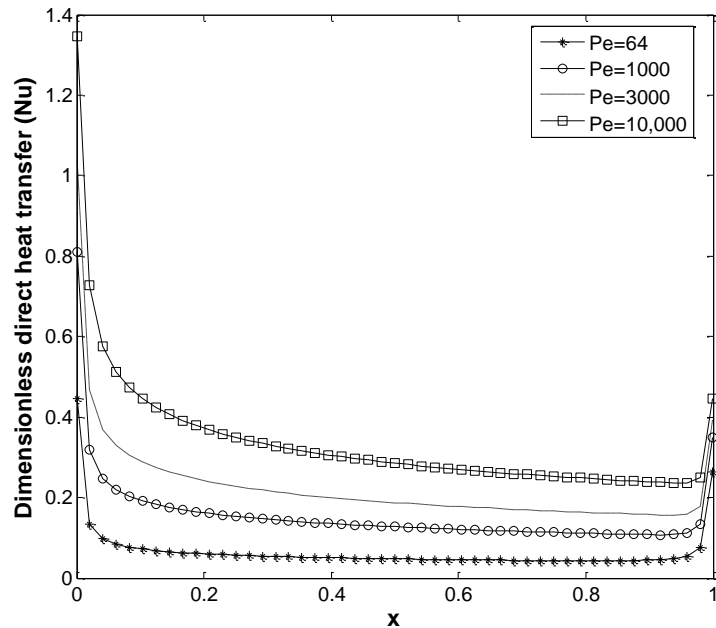
Figure 3-13- Non-dimensionalized heat transfer over the film at different *Pe* numbers, (water-silica), x=0 and x=1 are the leading and trailing edges of the hot-film, respectively.

A higher direct heat transfer rate is expected for strong fluctuations, as flow would carry away more heat from the wall. Leading and trailing edge singularity points show considerable heat flux in all range of *Pe* numbers.

After checking the code, we modeled single-element sensors, guard-heated sensors in a plane and guard-heated sensors on two planes. The design and fabrication of guard-heated sensors are explained in the following section.

3.5. New sensor designs and fabrication

3.5.1. Concept of guard-heated sensors in a plane

The difficulties mentioned earlier for single-element sensor usage can be removed or modified to some extent by new designs. Several designs have been suggested in order to overcome the deficiencies of classical thermal devices; we noted some of them earlier in this thesis. A few more new designs have been investigated and compared with the conventional thermal sensors in this study. The first device is made of two electrically separate heating elements including a sensor and a guard heater; a small central region which is considered as a sensor in a wall hot film is electrically isolated from the rest of the guard heater. Both the sensor and guard heater have the same thickness and are located on one plane parallel to the flow. Similar to the conventional thermal sensors, the long side of the guard heater is perpendicular to the direction of the mean flow. These two parts are maintained at the same temperature by two different anemometer circuits. The following figure illustrates the schematic of the probe:
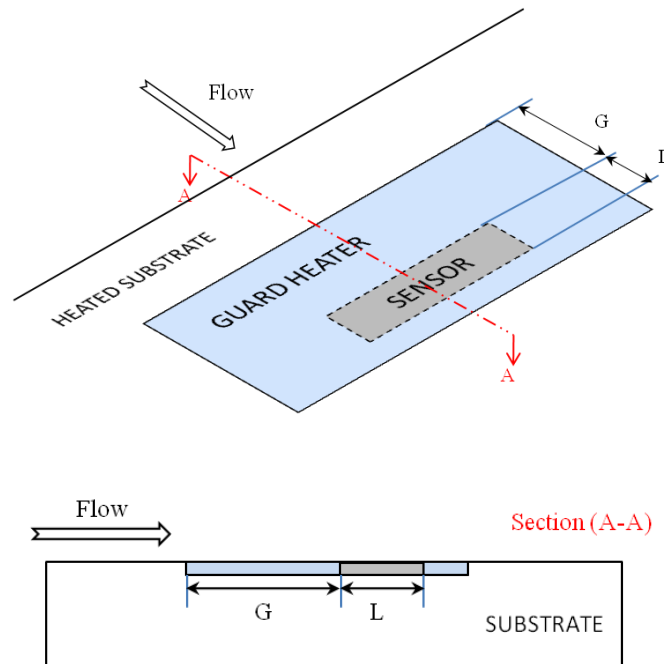
Figure 3-14- Schematic figure of the guard-heated sensor in a plane.

Even though the fluid still picks up heat from both the sensor and guard heater, the classical design would be modified in some ways. We expect streamwise and spanwise conduction in the fluid around the sensor to be considered as zero in all Pe number ranges, since there is no temperature gradient between the sensor and guard edges. The guard heater also acts to enforce a zero-temperature gradient sensor boundary, which prevents heat generated in the sensing element from diffusing into the substrate-fluid interface. By this means, heat from the current fluctuations in the sensor circuit does not spread over the surrounding interface before reaching the fluid, and the spatial averaging error will be reduced significantly. The effective heat exchange area for both single and guard-heated probes is calculated and compared in the results and discussion chapter. The guard heater would force most of the heat generated by the inner sensor to be released directly to the fluid, not the substrate. In this situation, the spurious amplification

caused by the heat reaching the fluid through the substrate is reduced. This sensor is studied in more details in Chapter 4.

3.5.2. Fabrication of guard-heated sensors in a plane

In terms of the fabrication process, guard-heated sensors in a plane need one more anemometer circuit in comparison to the single-element sensors to adjust the guard temperature. However, the multiple-element probes can encompass several inner sensors for two-component or multi-point measurements.

Four different guard-heated sensors in a plane have been fabricated in various sizes by R. Bhiladvala (2009) [25]. He created sensors of four sizes: 12×60 μm, 24×96 μm, 72×288 μm, and 250×1000 μm, ranging from 0.004 to 1.3 times the area of a commercial single-element WSS sensor made by DANTEC (55R46). In all the sensors, the sensing element is placed in the middle of a guard heater three times in size. The proper size can be used depending on the spatial scale of the flow structure. In addition, signal-to-noise ratio becomes crucial when the sensor is small. Thus, applying a bigger sensor is recommended, provided the spatial averaging restriction is met.

Six levels of photolithography patterning and deposition/etching were required using an oxidized silicon wafer with a silicon oxide surface layer, to make the sensor chip. An outline of the fabrication process is provided below:

1)   A thin dielectric layer of silicon oxide was grown on silicon base

2)   Four separate layers of gold bonding pad were evaporated on the substrate to provide current for the heating elements. Each pad was then attached to one end of a rectangular-shaped sensor and guard heater

3)   The gold layer was covered by a layer of silicon dioxide to electrically isolate it from the other layers

4)   Since the dielectric layer covers the whole area of the gold pads, two holes were etched through the silicon dioxide by using a lithography mask. The required electric current to provide a constant temperature in the guard heater was supported by these holes.

5)   The guard heater was created by evaporating a layer of nickel

6)   Another dielectric layer was deposited

7)   After the guard heater was deposited and attached to the gold pads, the connecting holes for the sensor were etched through two layers of silicon dioxide to reach the other two gold layers

8)   Another layer of nickel was created as a sensing element

9)   The last layer of silicon dioxide was then used to cover the sensing element

10)   At the end, to connect the gold bonding pads to the electrical section of the device, some connecting areas were etched

The chip was located on a ceramic holder by a central air cavity. Four connecting lead-wires were attached to the gold pads.

Figure 3-15- The guard-heated sensor chip, and the ceramic holder [25].

3.5.3. Guard-heated sensors on two planes

The other design which is investigated in this thesis is for guard-heated sensors on two planes in which a guard heater is applied beneath the sensor. This heating element is also kept at the same temperature as the sensor to block the heat loss into the substrate from the sensor.
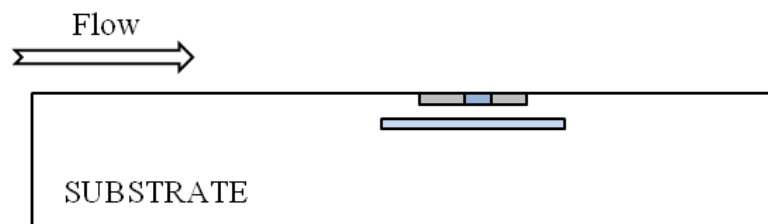
Figure 3-16- Schematic figure of guard-heated sensors on two planes.

The main problem in using guard-heated sensors is pre-heating which leads to lower direct heat transfer from the sensing element.

In addition to the fabrication process which is explained briefly in this section, the sensor performance with guard heaters both in the same plane and in two planes needs to be studied. Even though we are able to block the heat loss to the substrate, there are some

additional questions. Will raising the fluid temperature by the guard heater weaken the signal of the intended sensor leading to unacceptable signal-to-noise ratio? Are there other limitations? Other benefits of these two designs? Can we completely remove spatial averaging error? These questions are studied numerically and detailed results discussed in the next chapter.

4. Results and discussion

The principles of thermal wall shear stress sensors along with the limitations of conventional probes have been explained in the previous chapter. We showed that fabrication of multi-element guard-heated microscale sensors is feasible with the microfabrication technique. In this chapter, the performance of two new designs are presented based on numerical calculation; guard-heated sensors in a plane as well as guard-heated sensors on two planes are investigated in order to estimate how much of the substrate heat conduction error we can remove from single-element sensors by replacing them with any of the named designs.

We begin this chapter with a discussion of the single-element sensors on silica substrate (4.1), the effect of their sizes (4.1.1), and their effective heat exchange area (4.1.2). After presenting the restrictions of this type of probe, we study guard-heated sensors in a plane (4.2), and the rate of dimensionless direct and indirect heat transfer compared to conventional sensors (4.2.3). The location of the sensor within the guard heater (4.2.1) as well as the correlation between sensor and guard heater size is discussed thereafter (4.2.2). This is followed by a discussion about guard-heated sensors on two planes (4.3). All three designs are finally compared when the intended fluid for measurement is water (4.4). Since in many applications, such as aerodynamic design, the sensor is applied in air, we also research the probe behaviour in air with constant (4.5) and temperature-dependent (4.6) fluid properties. Finally, another material (silicon-silica) substrate is considered; the substrate which is applied for sensor fabrication explained in the previous chapter is simulated and compared with the silica substrate (4.7).

4.1. Single-element sensors

4.1.1. Performance of single-element sensors at various sizes

Heat transfer to the fluid and substrate from a single hot film, mounted flush on a conductive substrate (glass) is calculated. The portion of heat released to the substrate will subsequently transfer to the fluid; the upstream segment leads to preheating before the fluid reaches the sensor; thus direct convection from the hot element would be less than the Leveque solution, as Figure 4.1 indicates. Downstream heat exchange has a smaller value, since the fluid has already been heated by the hot film. This result shows good agreement with earlier published numerical calculations (see figure (4-a) from F.S. Tardu *et al*).

Recall that, in order to decrease the spatial averaging of fluctuations, it would be preferable to make sensors as small as microfabrication techniques allow; however, we would like to use a big enough sensor for the signal, related to direct heat transfer, to have a high signal-to-noise ratio. Therefore, different sizes can be used in different ranges of shear stress values and length scale of the fluctuations. Since different sensor lengths can be used for different measurements, we would like to know if the scaling of similarity parameters Nusselt number (Nu) and Peclet number (Pe) obtained for the Leveque problem (zero heat conduction) can be applied to the conventional single element sensor with substrate heat conduction. Will a relation of the form ($Nu = A \, Pe^{\frac{1}{3}} + B$) still apply? If so, will the constants vary appreciably with sensor length (L)? To test this, the numerical model was run to obtain the heat transfer for three single-element sensors of different lengths L, with results shown in Figure 4-1 below.
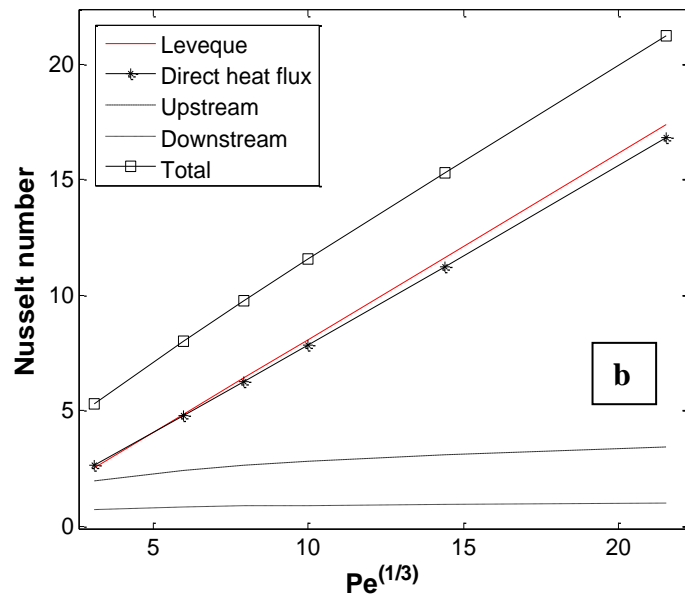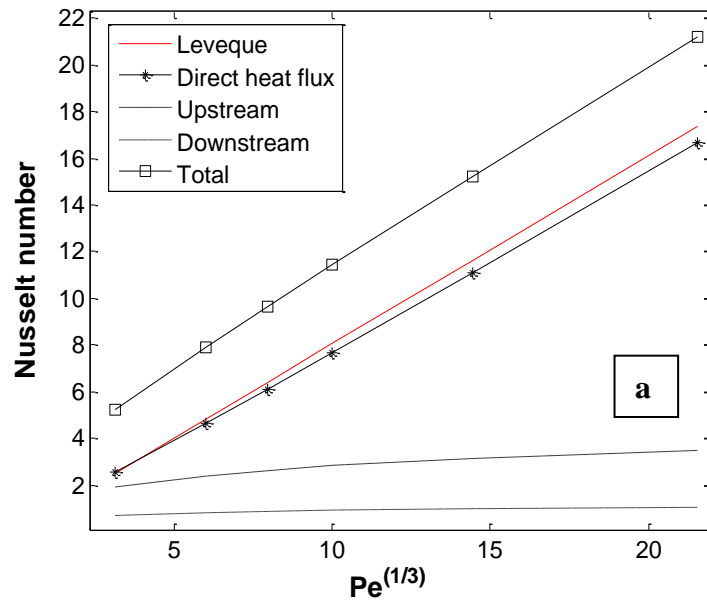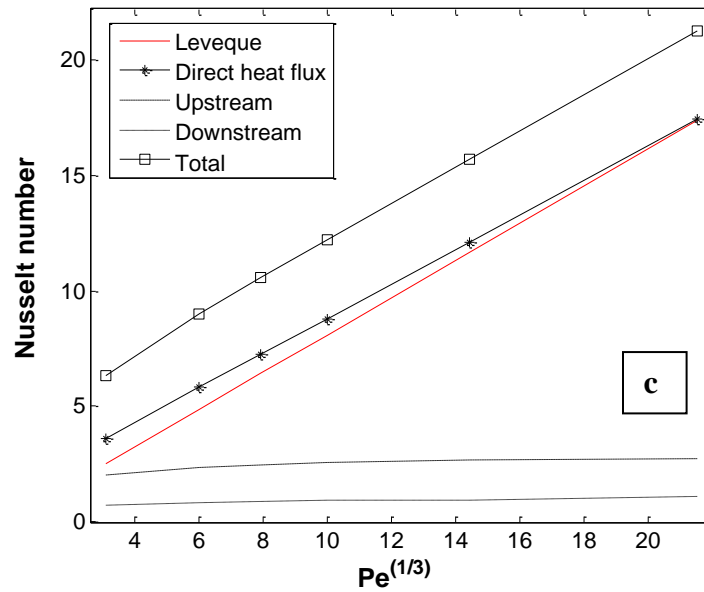
Figure 4-1- Nondimensional plots of variation in heat transfer (Nu) with applied shear (Pe) for three different sensor sizes a) $L = 36\mu m$ b) $L = 24\mu m$ c) $L = 2\mu m$.

All the figures indicate consistent behaviour for all the sizes in single-element sensors located on the silica substrate. Total dimensionless heat transfer from the interface are nearly the same for $L = 24\mu$m and $L = 36\mu$m, which indicates that Nu, Pe continue to be useful similarity parameters for this problem as well. The $Nu - Pe$ relation for total heat transport for each case is indicated in the following equations. Two bigger sizes show almost the same slope, which indicates signal strength, as well as constant terms. The smallest size at low Pe numbers shows the highest rate of diffusion to the surroundings.

$$For\ L = 2\mu m \quad \rightarrow \quad Nu = 0.80Pe^{1/3} + 4.0$$

$$For\ L = 24\mu m \quad \rightarrow \quad Nu = 0.86Pe^{1/3} + 2.8$$

$$For\ L = 36\mu m \quad \rightarrow \quad Nu = 0.87Pe^{1/3} + 2.7$$

It is found that Nu numbers calculated based on direct heat transfer from the sensor are also nearly identical for the two bigger sizes. However, the far smaller size ($2\,\mu m$) shows significant difference in comparison to the other sensors, as well as the highest deviation from the analytical solution. The reason for the increased direct Nusselt numbers for the small sensor size can be described by the ratio of perimeter and internal area. Smaller sensor lengths increase the ratio of hot film perimeter to area. Therefore, the amount of heat released to the surroundings, which causes axial conduction in the fluid, becomes more consequential at low Pe, as seen in the figure. An experimentalist plotting the results of a calibration with a large single-element sensor therefore sees that calibration data plotted as Nu vs $Pe^{1/3}$ is usually well approximated by a straight line. This appears to provide some validation, and may build confidence in the accuracy of experimental data from a single-element probe –this confidence is misplaced, as may be seen below.

Heat diffusion to the surroundings makes the heat exchange area for the sensor (effective size) bigger than its physical size, and causes spatial averaging. How can we estimate the effective size of the sensor? How is this size affected by the thermal properties of the fluid?

4.1.2. Conductive wall influence on effective heat exchange area in single-element sensors

One main problem of conventional sensors is spatial averaging, as discussed in Chapter 3. For this reason, we need to use a small sensor for a better resolution. It remains to be seen whether making a physically small sensor can remove this error. Recall that, a conducting wall would affect the physical sensor size. As we showed in the

temperature contour in Chapter 3, temperature does not change uniformly along the interface in either the upstream or downstream direction; temperature gradient and subsequently heat transfer to the fluid is much higher, close to leading and trailing edges of the hot film, than at a distance away from them. Thus, defining the effective heat exchange area based on a length over which the minimum temperature has a specific value does not look reasonable. We propose the definition of another parameter named the equivalent length which is related to the influence of a conducting wall on the effective heat exchange area. For a fair comparison, an equivalent length can be defined by using the Leveque similarity solution. We define, the length L_{eq} of a hot-film for which the analytical Leveque solution would yield the same heat transfer rate from the fluid-solid interface is taken to be the same as that from compared to the situations that Leveque assumptions are applied.

$$Nu_{Lev} = Nu_t \quad \rightarrow \quad 0.807 \, Pe_{eq}^{1/3} = \frac{hL_{eq}}{k}$$

<div align="right">**Eq. 4-1**</div>

The convection coefficient can be obtained by upstream heat transfer per unit depth.

$$q_t = hL_{eq}(T - T_\infty)$$

<div align="right">**Eq. 4-2**</div>

Note that Nu_t and q_t are associated with total heat flux to the fluid, including upstream, downstream and the sensor itself. Substituting Equation 4-2, and $Pe_{eq} = \frac{SL_{eq}^2}{\alpha_f}$ into Equation 4-1, followed by normalizing the length according to hot film length gives the following relation, which scales the equivalent length as $Pe^{-1/2}$.

$$\frac{L_{eq}}{L} = Pe_L^{-1/2} \left[\frac{q}{\Delta T. k_f. 0.807} \right]^{3/2}$$

<div align="right">**Eq. 4-3**</div>

This equation can be rewritten by substituting $Pe_L = \frac{SL^2}{\alpha_f}$:

$$L_{eq} = \left[\frac{q \, \alpha_f^{1/3}}{0.807 \, \Delta T \, k_f S^{1/3}} \right]^{3/2}$$

Eq. 4-4

Nu_t in Equation 4-1 is obtained by numerical calculation along the solid-fluid interface. The effective length of several single element sensors on silica substrate- 36μm, 24μm, 2μm- used in water and air are shown in figure 4.2.a and 4.2.b.
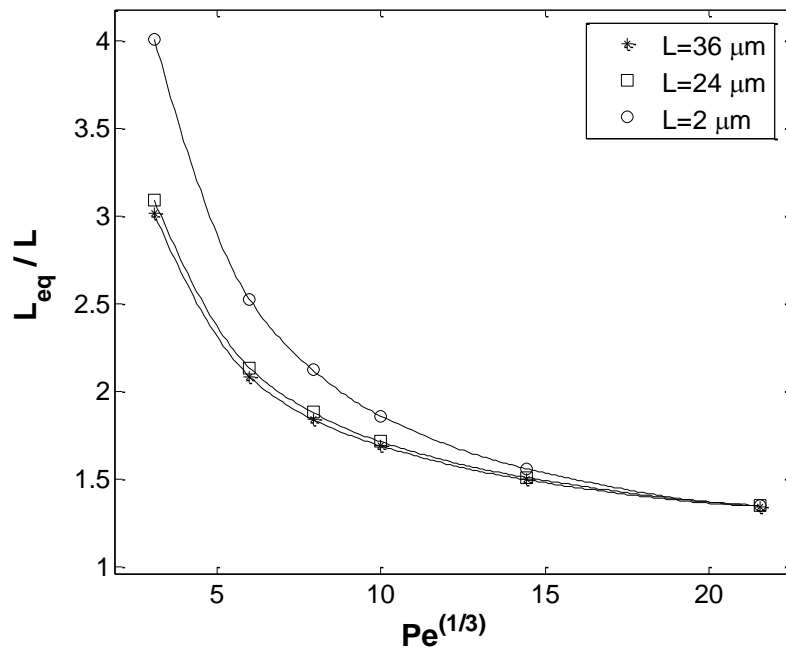
Figure 4-2-a) Sensor equivalent length is seen to be 1.5-4 times the physical sensor length as Pe varies from 30 to 10,000 (silica-water). The ratio increases as sensor size decreases.
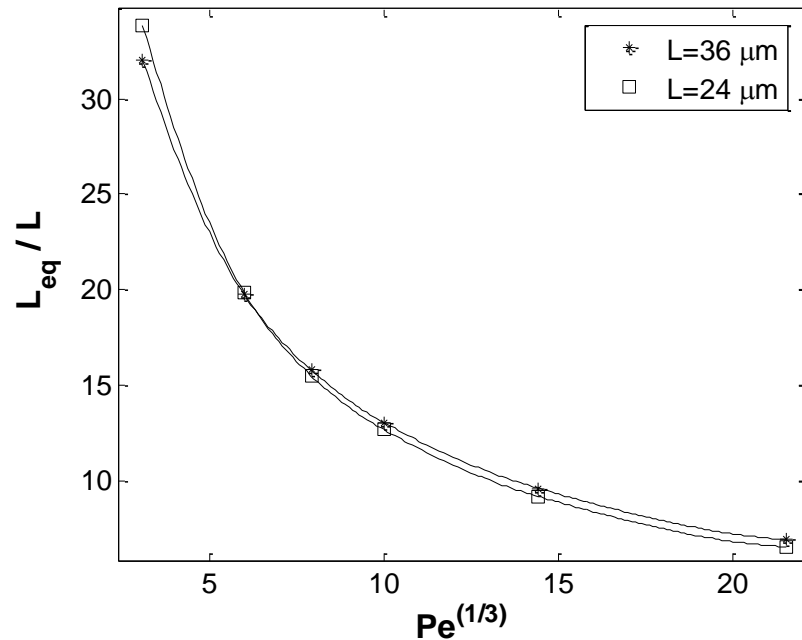
Figure 4-2-b) Sensor equivalent length is seen to vary from 6.5 to 33 times the physical sensor length as Pe varies from 30 to 10,000 (silica-air). The ratio increases as sensor size decreases.

As figures 4.2 show, spatial averaging error is not ignorable even for small sensor sizes; the equivalent length of the smallest sensor is about 4 times bigger than its actual physical size at $Pe = 30$ in water. This ratio decreases for two other bigger sizes. Higher values of shear stress reduce the heat exchange area. This fact can be used to explain why the ratio of L_{eq}/L for all three cases reaches the same value at the highest Pe number.

One can see that, effective spatial resolution varies dramatically with shear stress magnitude for single-element sensors. Even by making a small sensor we would not be able to improve spatial resolution. This deficiency is much higher in gases, which have lower thermal conductivity than water.

The same type of results are shown for two sizes $L = 36\mu$m and $L = 24\mu$m in air; in this case, the equivalent length is over 30 times the physical length, which is 10 times

higher than in water. Even at high Pe numbers, L_{eq}/L is more than 5. All these results indicate the significance of spatial averaging error in single-element sensors. Attempting to use the same probe in air and water results in vastly different spatial averaging errors in the two cases.

This fact also explains why fluctuation strengths are very low for air compared to all other DNS calculations or experiments as reported in the following table:

Table 4-1- Measurements of $\tau_x^{'}/\tau$ [19]

Chambers *et al.* [20]	Channel	Hot film	Air	0.06
Thomas [27]	Boundary layer	Hot film	Air	0.12
Eckelmann [28]	Channel	Hot film	Oil	0.24
Madavan *et al.* [29]	Boundary layer	Hot film	water	0.24
Mitchell and Hanratty [14]	Pipe	Mass transfer	Water	0.32
Mao and Hanratty [30]	Inverse method	-	-	0.37
Yoshino *et al.* [31]	Channel-DNS	Hot film		0.33-0.4
Kim *et al.* [32]	Channel	Numerical sim.	-	0.36

The rms values obtained with hot films in a wind tunnel indicate the effect of low thermal conductivity of air on sensor response in comparison to those obtained with other techniques in water. Dengel *et al.* (1987) reported that the substrate material affects the measured rms value significantly [33].

The results of this section prove the influence of conductive wall on the sensor is not ignorable. The application of the single-element sensor in air, for applications such as wind turbines, would be absurd, unless the substrate conduction errors are strongly reduced. In order to do so, the design of conventional sensors needs to be modified. Using the guard heater increases the functionality of the probe. Finding the performance

of a guard-heated sensor as well as its optimum design are the focus of the results that follow.

4.2. Guard-heated sensor in a plane:

4.2.1. Maximizing direct heat transfer from a guard-heated sensor in a plane

Our primary goal in the design of guard-heated sensors is maximizing the ratio of direct to indirect heat transfer. For more clarification of direct and indirect heat transfer, heat distribution from a heated film in a guard-heater is indicated in figure 4.3

$$Q_{Id} = \sum_{j=1}^{n} Q_{Id(j)}$$
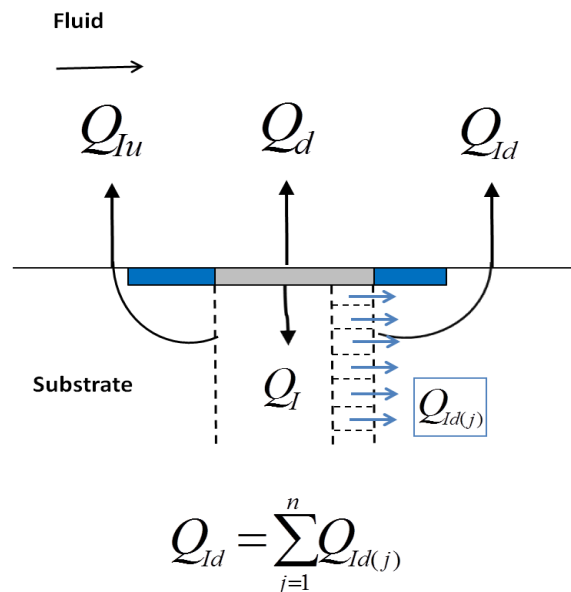
Figure 4-3- Direct and indirect heat transfer to the fluid from the sensing element. Grey and blue rectangles indicate the sensing element and guard heater, respectively.

As shown in the figure, the conducting wall transfers some portion of generated heat in the sensor to upstream and downstream directions. These are the indirect upstream and indirect downstream heat transfer components, named Q_{Iu} and Q_{Id}. Convective direct heat transfer, named Q_d should ideally be the sole basis of the current change causing our signal. Since the substrate is isolated in all boundaries except in the interface with fluid,

the sum of Q_{Iu} and Q_{Id} represents indirect heat transfer, Q_I. Q_{Iu} and Q_{Id} can be obtained by integrating heat transfer along a line perpendicular to the intended hot film, shown in the Figure 4-3 by the left and right vertical dashed lines, respectively.

As we showed in Chapter 3, preliminary prototypes of different sizes of thermal sensors have been fabricated in a supporting guard three times bigger than the sensing element. All the sensors are located at the center of the guard. Having established the feasibility of fabrication, we would like to know how this sensor location within the guard and 1:3 ratio of sensor length to guard length affects device performance –the ideal case would be zero indirect heat transfer and $L_{eq} = L$.

The main question in two-element sensor design is the best location of the sensing element centre within the guard heater, for closest approach to this ideal case. Another question which arises is whether this "best location" depends on the magnitude of the shear stress. If it does, the sensor can only be used accurately in a small range of fluctuations, which poses difficulty in turbulent flows. The intuitive simple picture that the guard heater need only impose zero temperature gradient around the sensor edges, to block substrate heat conduction, suggests the location and size of the guard can be chosen arbitrarily. Is this true?

Our results in figure 4.4 show that there is a small portion of the film in which conduction to the substrate would be close to zero, since the film-substrate heat conducted splits in two upstream and downstream directions from the leading and trailing edges, respectively. For a small sensing element located in that region, we found that almost all the heat goes directly to the fluid.
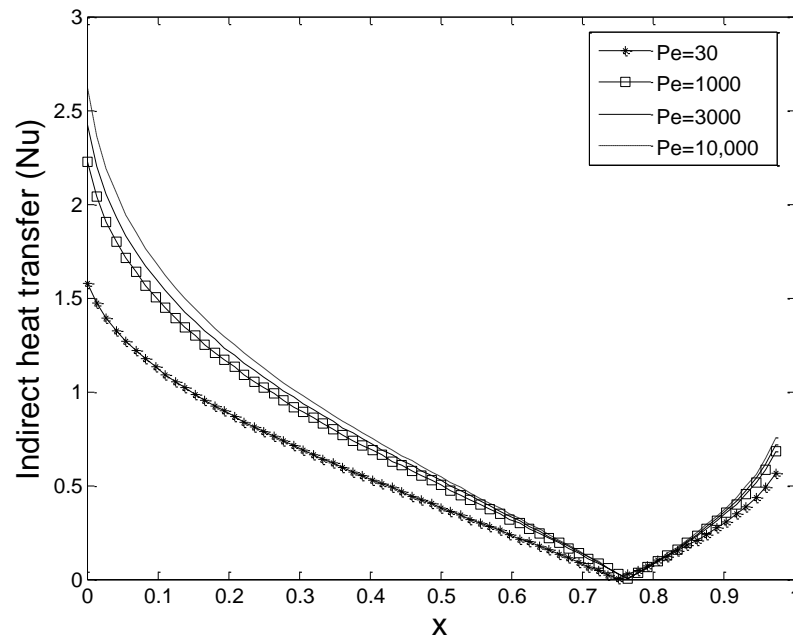
Figure 4-4- Undesirable indirect heat transfer from hot film, (water-silica), x=0 and x=1 are the leading and trailing edges of the guard heater, respectively.

As is clear from the figure, locating a small sensor centered at $x = 0.75$ would remove undesirable heat loss to the substrate significantly when water is used as the fluid. This location does not change considerably over a large range of Pe numbers. Thus, we would be able to fix the location of the sensor in dynamic flows. Application of this type of sensor can be reliable in turbulent flows in which the local wall shear stress changes rapidly. Thermal conductivity of the fluid changes the sensor location by affecting heat exchange between solid and fluid. We also studied air as a gas having low thermal conductivity, and found the appropriate location moves about 10% towards the leading edge. In this case, the suitable location moves slightly depending on the Pe number. This issue is discussed in more detail in section 4.5.

According to our results, the sensor location cannot be fixed for all the intended fluids. This fact puts some limitations on the device application, since a design for a

specific fluid would not be applicable to another fluid with different properties. Due to the fact that interest in common fluids water and air flow is the strongest, a different design can be used for each of these two cases.

4.2.2. Correlation of guard heater to the sensor size

After finding the best location of the sensor in the supporting heating element, we must determine whether the guard-to-sensor length ratio is relevant in designing a guard-heated sensor in a plane. One can attempt to make a very small guard heater around the sensor to block the heat diffusion, as well as minimize the undesirable effect of preheating. How would this perform? What would be the deficiency of such a design?
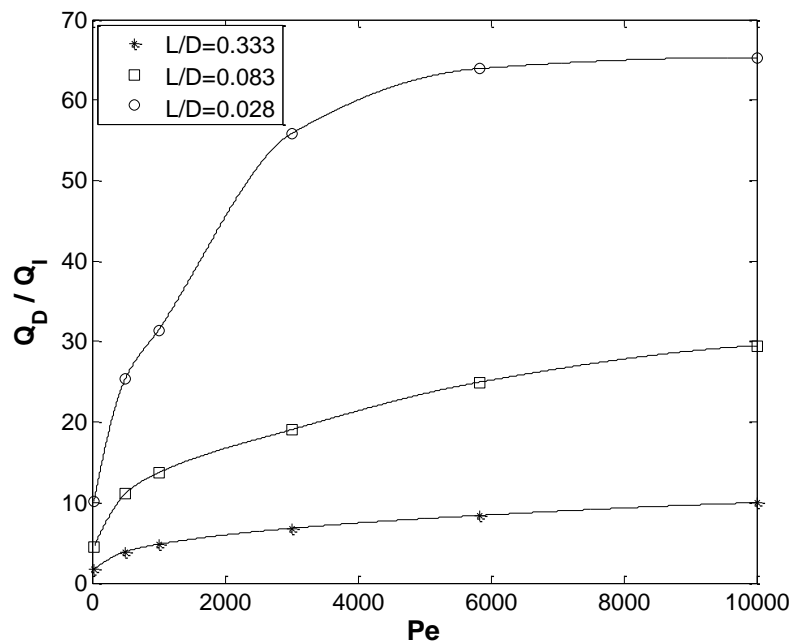
Figure 4-5- Direct heat transfer per indirect conduction in the substrate, L/D represents the sensor length as a fraction of length of the guard heater.

Figure 4.5 shows the ratio of hot film-fluid heat transfer to dissipation in the solid for various proportions of sensor-guard heater lengths. It shows how the device performs if

we locate the sensor at the best location in the guard heater and change the ratio of sensor to guard heater length. The smallest L/D ratio has the highest rate of direct heat transfer per undesirable indirect heat transfer, which makes a small L/D ratio generally more suitable for measuring shear stress. As the guard heater becomes shorter, more heat from the sensor is extracted to upstream and downstream directions, especially at low Pe numbers. The reason for significant increase in Q_D/Q_I for L/D=0.028 is related to the small size of the sensor. As the sensor becomes smaller, and place at the best location, the indirect heat transfer would dramatically decrease. In addition, a small movement of the sensor in the guard heater significantly changes the rate of Q_D/Q_I. According to these results, choosing a small guard heater would not remove the errors associated with the conducting wall. However, Fig 4-5 shows that when substrate conduction cannot be completely eliminated, such as at low Pe, a small guard heater may lose a significant fraction of heat through the substrate.

In brief, the sensor performance can be enhanced by choosing the right location and length of the sensor, as we discussed. One concern that needs to be addressed is the extra heat released by the guard-heater element run by a separate circuit, which pre-heats fluid over the sensor and reduces the amount of direct heat transfer from the sensing element to the fluid, leading to a reduced signal strength. Would the reduction of some errors such as spatial averaging be acceptable in comparison to losing the signal strength?

4.2.3. Direct and indirect heat transfer from guard-heated sensors in a plane

The rate of direct heat transfer as well as its proportion to indirect heat transfer is required for a trade off between losing signal strength and eliminating the errors. We note first that pre-heating of fluid also occurs with the unguarded single element sensor – however the energy used in this pre-heating comes from the single sensor element itself, and is incorrectly attributed to a non-existent "slow" shear stress fluctuation. As we showed in Chapter 3, the large temperature gradients at leading and trailing edges of the hot film cause a large amount of heat transfer. These two regions are not a part of the sensing element when the sensor is surrounded by a guard heater. Therefore, in comparison to guard-heated sensors, single element sensors show a higher direct heat transfer, and stronger signals –but the increase of signal contributes mostly to a spectral distortion error, which is a spurious increase in the spectral value at the "slow" or low-frequency end.

Single and guard-heated sensors have been compared under the same conditions to anticipate sensor response. Direct heat transport from two sensors ($L = 24\mu m$, $L = 2\mu m$) used as single-element and also as guard-heated sensors, with sensing element located appropriately within a guard heater three times bigger, is indicated in figure 4.6 for water.
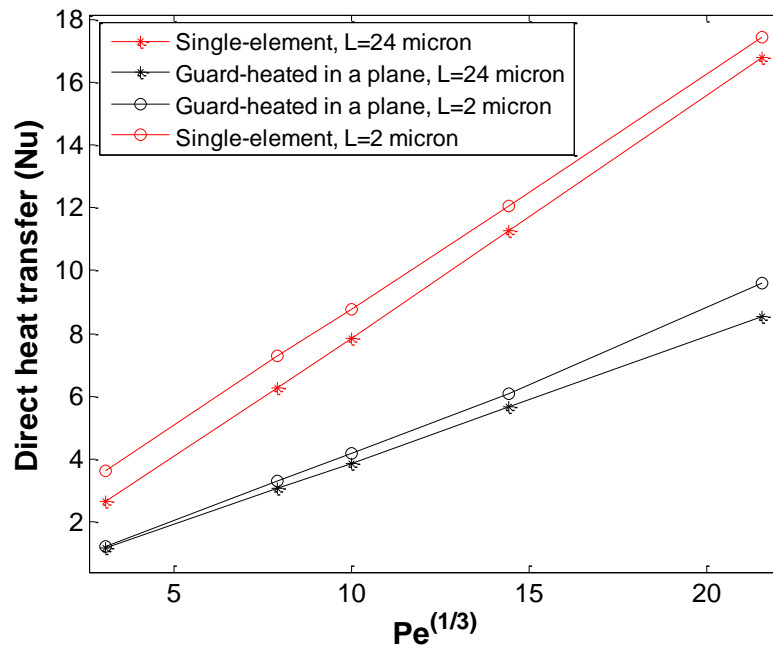
Figure 4-6- Non-dimensionalized direct heat transfer to water from single-element and guard-heated sensors in a plane. The difference in values between the single and guard-heated sensor of each size contributes mostly to an error -a spurious increase of the low frequency end of the measured WSS spectrum.

Even though this figure indicates higher direct Nu numbers for single-element probe– almost twice as high as the guard-heated sensor– we should consider this difference as an error in conventional devices; their signals express direct heat transfer as well as total heat loss to the substrate. Recall that, signals received by a single-element probe include spurious amplification in small shear stress. Spurious amplification caused by the conductive substrate can be diminished using a guard heater, since sensor-to-substrate heat transfer would be lower. Consequently, higher values of Nu numbers as well as the $Nu - Pe$ slope of single-element sensors do not represent better performance of the device. For convenience of fair comparison, we would like to calculate what ratio of total generated heat in the sensing element is associated with direct heat transfer to

fluid. Conversely, since we are using another heating element, the signals should be strong enough to be recorded.

The fraction of total heat loss from the sensor (resistive heating, I^2R) that is directly transferred to fluid is shown in the following figure. All the sensors are embedded at the best location within guard heaters three times bigger than the physical sensor length. The substrate is made of silica.
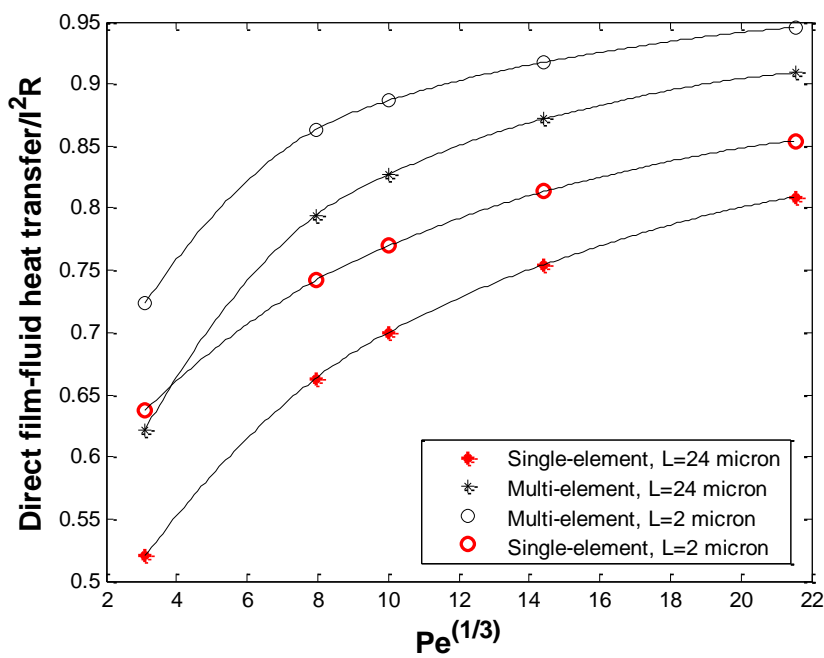
Figure 4-7- Fraction of total heat generated I^2R that is transferred directly from sensor film to water (guard heater lengths are three times bigger than the sensors).

Our results thus far show the fraction of direct film-to-fluid heat transfer to the total heat generated in the sensing film can be increased by around 10% when a guard-heated sensor is applied. Since diffusion to the substrate is reduced by using the guard heater, a larger portion of total generated heat in the sensing element releases to the fluid. Therefore, the measured signals are more associated with the given wall shear stress,

especially for small hot films measuring strong fluctuations; the sensor with 2μm length only suffers from a 5% heat conduction to the solid at $Pe = 10,000$.

4.2.4. Dependency of sensor response to wall temperature in dynamic flows

Despite the fact that the guard heater increases fluid temperature, the temperature ahead of the sensor would not vary extensively. In conventional devices, this temperature changes in a large range as the Pe number varies. This issue is important in turbulent flows as the fluctuations change rapidly. The correlation between the fluctuation and fluid temperature before the sensor cannot be easily determined. Slow fluctuations leave the substrate at a comparably high temperature, which still can influence the fluid regardless of the next fluctuation strength; this is due to the high thermal inertia of the substrate. We would expect to uniform the fluid temperature and decrease some errors due to the substrate thermal inertia by using supported hot film. However, given that the temperature rises slightly using a hot film around the sensor, the sensor response is more reliable in dynamic flows. In order to clarify some of these concerns, we have shown the fluid temperature behavior for different devices.
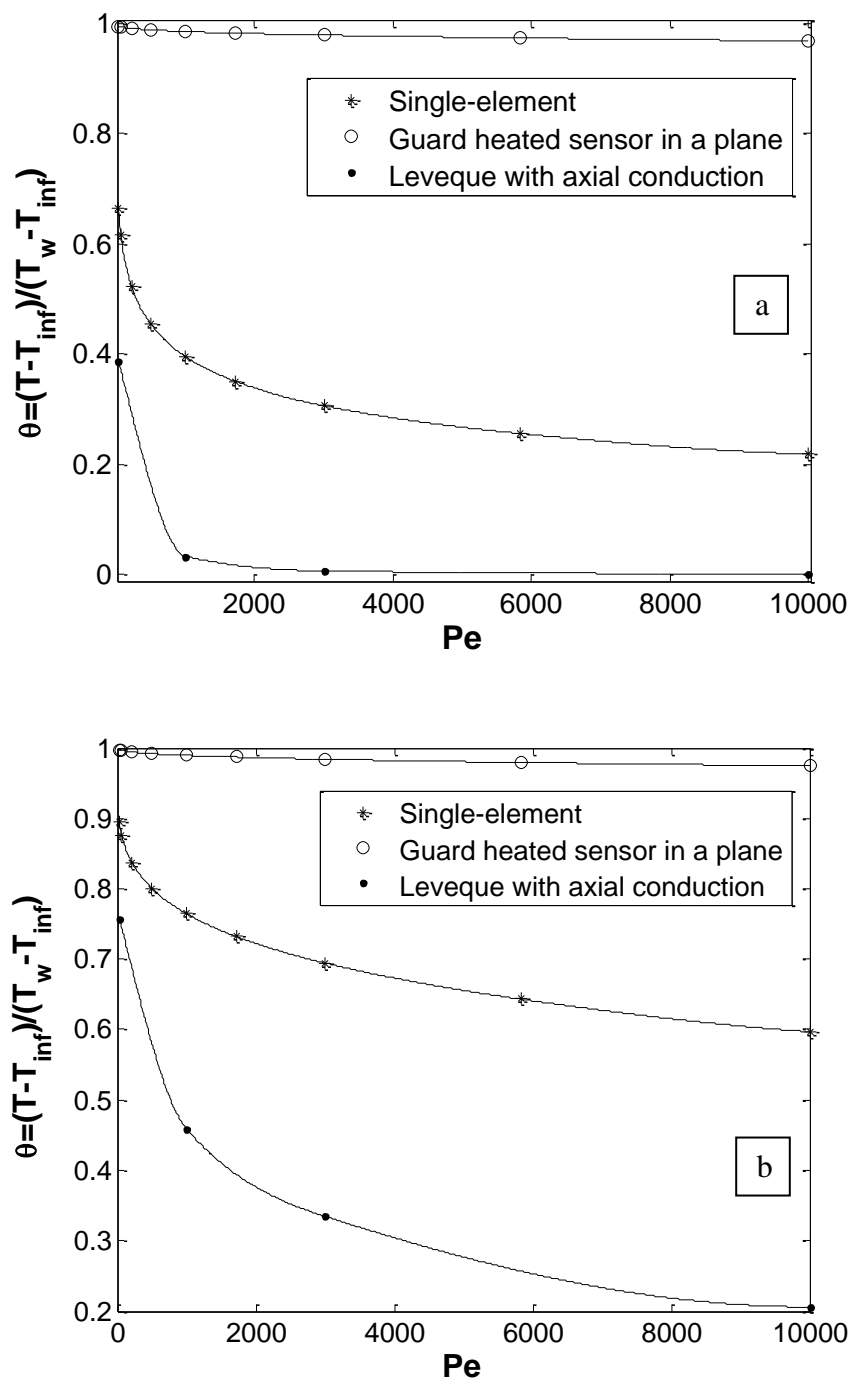
Figure 4-8- Dimensionless fluid temperature ahead of the sensor a) Δx=0.0115L, Δy=0.003L b) Δx=0.010L, Δy=0.003L from the sensor leading edge- (silica-water).

These figures show the fluid temperature right ahead of the sensor, $\Delta x = 0.01L$ and $0.0115L$ $, \Delta y = 0.003L$ away of the sensor in three cases: single-element, guard-heated sensors in a plane, and our simulation of the Leveque solution. In the theoretical Leveque solution the fluid temperature in the whole area in the upstream direction should be at ambient temperature. The axial conduction in the fluid was not kept at zero in our calculations due to code restrictions. Therefore, we can see the temperature variation in the Leveque solution, which is less than the other cases, even though the substrate influence is removed. Dimensionless temperature for the single-element sensor varies between 0.6 and 0.9 for Pe numbers ranging within 30 and 10,000. In a guard-heated device, this temperature is almost at a constant value near the hot film temperature. Even though the temperature in the guard-heated sensor is high, it shows almost a constant value which can be considered as favorable; the fluid temperature very close to the sensor does not change based on the current or former fluctuation. Thus, the substrate dependency can be lowered to some extent. The main concern in applying guard-heated sensors is signal strength. Signals will be ruined by noise in the system if the signals are not strong enough. For a small value of voltage ($V = 5 \times 10^{-3}$) a minimum rate of $Q \cong 2.5 \times 10^{-6}\, W$ from the sensor would be required when nickel is used as the sensing element. We have computed the heat transfer rate from the smallest guard-heated sensor in the lowest Pe number (Pe=30). For sensor ($L = 2\mu m, W = 8\mu m$) within a guard heater three times bigger in a plane, the amount of heat released to the fluid directly is around $Q \cong 232 \times 10^{-6}\, W$. This rate of heat transfer can be easily recorded by the device.

4.3. Guard-heated sensors on two planes

The results related to guard-heated sensor in a plane indicate that there is remains a small rate of indirect heat transfer. Can we keep the undesirable indirect heat transfer to be zero by another design? To answer this question we have analyzed a device with a guard heater beneath the sensor to check direct sensor heat transfer, and the effect of a second hot film on fluid temperature. A thin layer of silica is sandwiched between two hot films; the second hot film is slightly bigger. More details about this design have been explained in Chapter 3.

The presence of a guard-heating element beneath the sensor is in order to have better control over the conducting wall. There are two competing effects associated with this change. The heat released upstream from all the heating elements could diminish direct heat transfer. On the other hand, since indirect heat transfer is more controlled in this design, a smaller fraction of the heat generated within the sensing element would be lost through substrate conduction, as desired. We investigate this question numerically.

4.3.1. Indirect heat transfer from a guard-heated sensor on two planes

For the guard-heated sensor in a plane, we found the best location of the sensing element. The location is also a question for guard-heated sensors on two planes. In order to do so, indirect heat transfer to upstream and downstream through the substrate is calculated when a second hot film is used under the sensor.
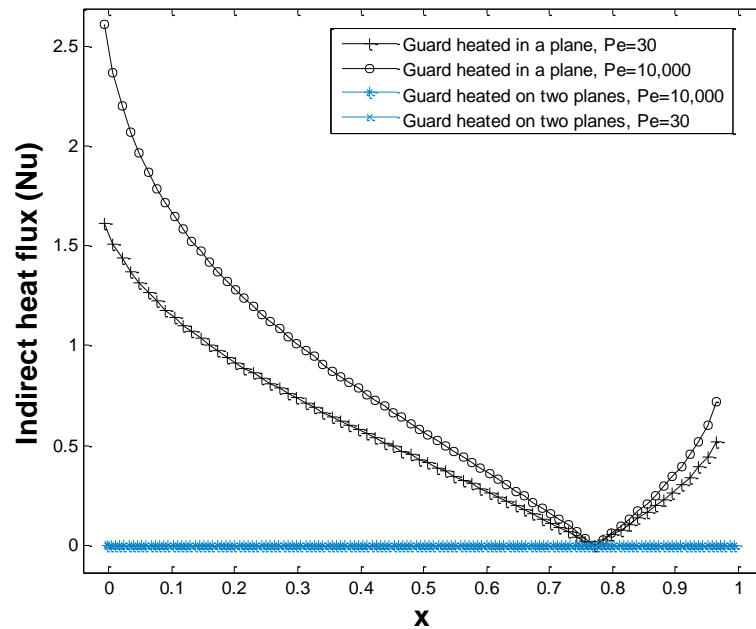
Figure 4-9- Dimensionless heat transfer from hot film to the substrate for a guard-heated sensor on two planes. x=0 and x=1 are the leading and trailing edges of the guard heater, respectively.

As the graph shows, the conduction term is blocked almost entirely along the hot film except the edges of the sensor; the sensor surroundings can also be protected by another guard-heater. Although the direct sensor heat transfer is reduced, we are able to remove some errors such as spatial averaging.

In order to control spatial averaging completely, we have used one more guard heater around the sensor in addition to the heating element on a lower plane. Hence, the guard-heated sensor on two planes made of three electrical heating elements is studied and presented in the next sections. The two guard elements can be run on a single anemometry circuit.

The performance of all the named sensors is compared in the following section in terms of direct heat transfer and spatial averaging errors.

4.4. Three designs comparison

Direct, upstream and downstream non-dimensionalized heat transfer for a range of shear stress is compared in following figures. Upstream and downstream heat transfer in a single element device can be found from the interface at areas of interest, since the boundaries at three ends of the solid are chosen to be adiabatic. Thus, the generated heat in the sensing element will transfer into the fluid through the interface. In guard-heated devices, the rate of heat exchange at the interface includes the sensor and guard-heater heat loss, which complicates assessment of the heat loss only from the sensor, not the protective heater. In order to estimate the indirect heat transfer rate, two planes at leading and trailing edges of the sensor perpendicular to the fluid direction are defined. Total heat transferred through the leading edge plane, from the solid region beneath the sensor toward the upstream, shows the amount of pre-heating from the sensor itself. The opposite heat transferred from the plane at trailing edge indicates the segment of heat loss to downstream.
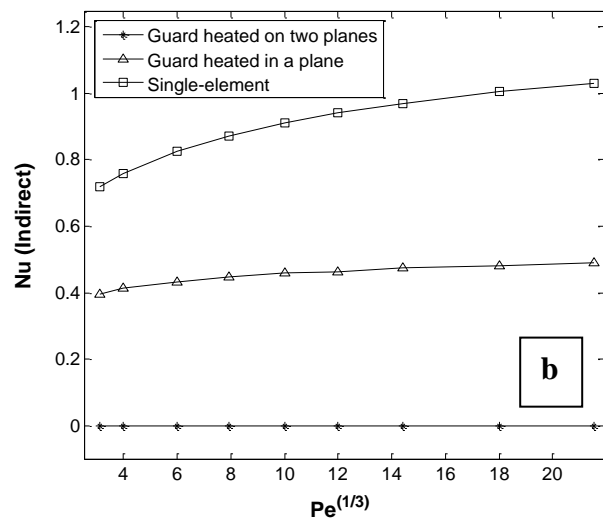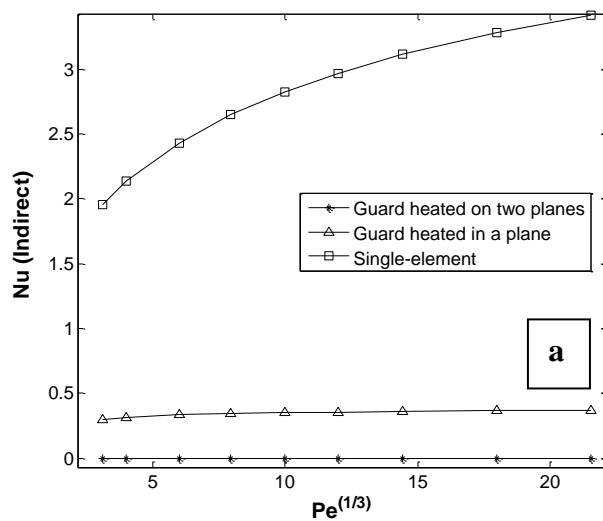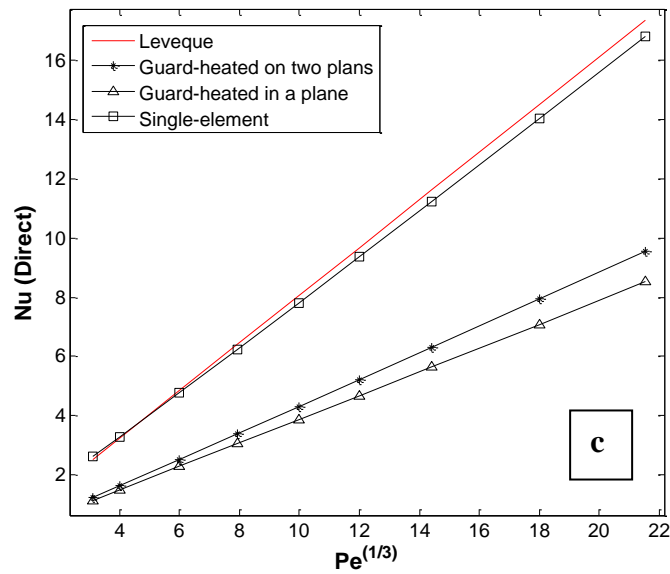
Figure 4-10- Upstream, downstream and direct dimensionless heat transfer from single-element, guard-heated sensor in a plane and guard-heated sensors on two planes a) upstream indirect b) downstream indirect c) direct.

Direct Nu number comparison shows the single-element device has the highest dimensionless direct heat transfer rate when compared to the other two designs, as less pre-heating is involved. Both guard-heated sensors have almost the same behaviour in small fluctuations; however, the sensor, made of two guard heaters, has a slightly higher slope than a two-element sensor. The conventional sensor also showed the strongest signal strength. Direct dimensionless heat transfer of one and two guard-heated sensors ($L = 24\mu m$) at fast fluctuation ($Pe = 10,000$) have 50.9% and 44.9% deviation from the Leveque solution, respectively.

The main point we can mention here is the reduction of indirect heat transfer. Upstream Nu numbers for two element sensors are less than 20% of the single- element sensors. These values as well as downstream Nu are zero when the guard-heated sensor on two planes is used for the whole range of applied shear stress. This fact is crucial, as it

removes many limitations in conventional sensors as well as making the signals more reliable.

Finally, the equivalent lengths of all the three designs are compared in this research. The effective heat exchange area was calculated in comparison to the Leveque solution. As we already mentioned, the heat flux rate should be compared with the equivalent amount of heat released from the sensor when the Leveque assumptions are applied (see Equation 4-4).
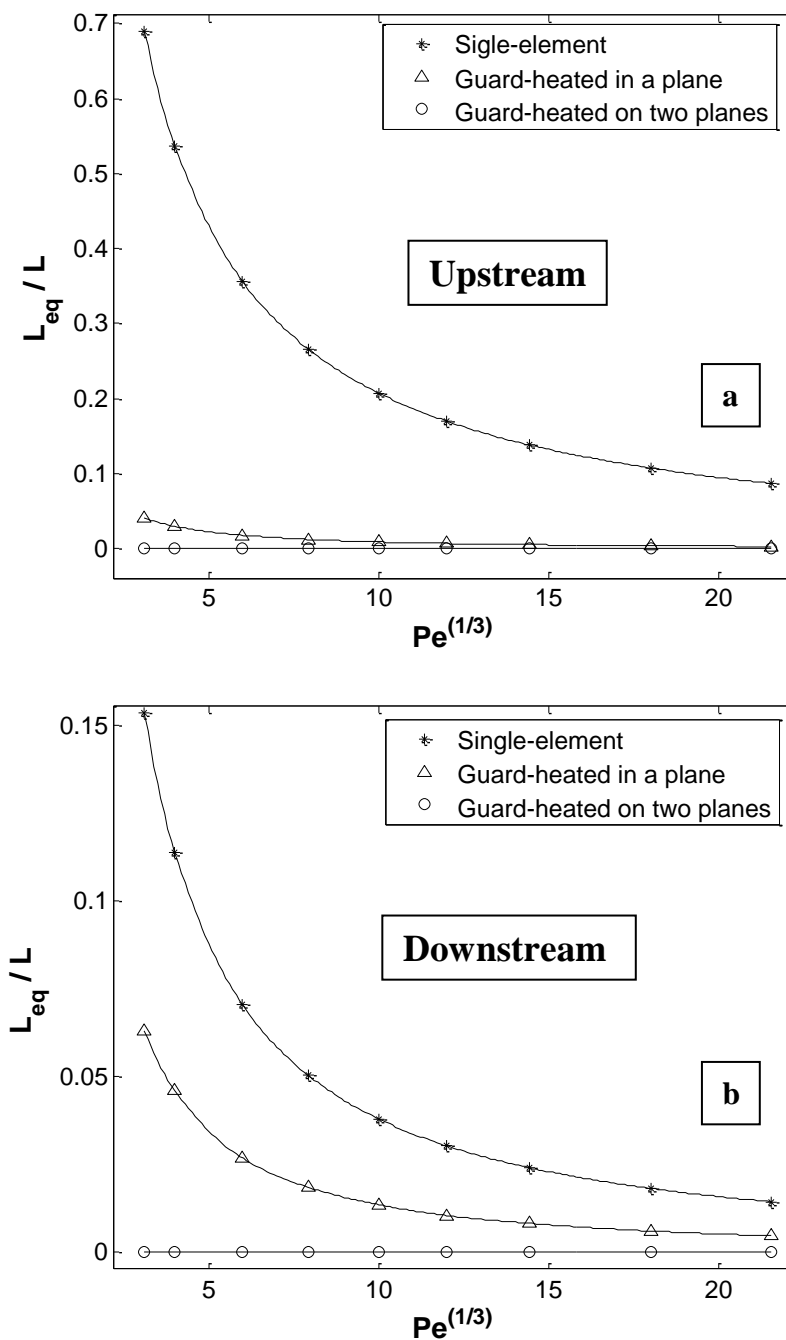
Figure 4-11- Equivalent length (L$_{eq}$) per sensor length (L) of single-element, guard-heated in a plane, and guard-heated on two planes sensors for a) upstream, and b) downstream.

As Figure 4.11 shows, one-element upstream L_{eq}/L is approximately 14 times bigger than the guard-heated sensor in a plane at the lowest Pe number, in which natural

convection plays an important role. This ratio leans toward zero for the guard-heated sensor in a plane at $Pe = 10,000$. The downstream L_{eq}/L difference for these two designs is smaller at the range of intended shear stress.

We found, since the guard heaters at the guard-heated sensor on two planes prevent heat loss from the sensing element to the upstream and downstream, these equivalent lengths are zero. Thus, in this design, the signals taken from the sensor are only related to the current shear stress, not the heat loss to the substrate. This advantage makes this sensor more reliable than the other designs.

So far, the limitations of single-element sensors have been reviewed, and two new designs to overcome these restrictions have been studied. The performance of all three designs has been investigated and compared in water. However, the sensor behavior would be different in contact with other fluids, especially in a gas with low thermal conductivity such as air.

4.5. Wall shear stress measurement in air

4.5.1. Constant fluid properties

Having knowledge of lift and drag force and the separation point has been an interest in aerodynamic designs for decades. Reducing drag force on devices in contact with air including wind turbines or aircraft can be actively controlled by measurement of shear stress on the solid surface. In this section, we study the sensor response applied for wall shear stress measurement in air.

The first step was obtaining the amount of direct heat transfer for a range of shear stress. Fluid properties are assumed to be independent of temperature. The effect of temperature-dependent properties of air is studied in section 4.6.
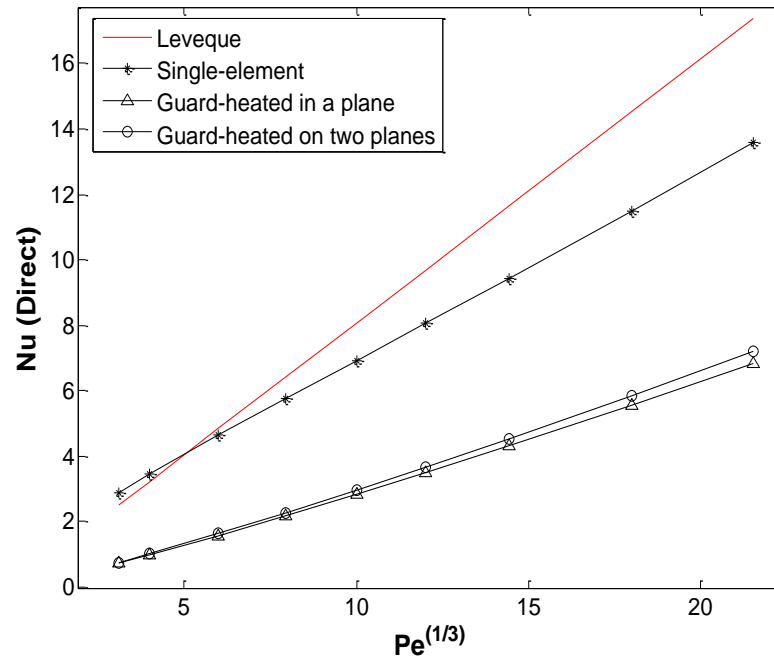
Figure 4-12- Direct heat transfer from single-element, guard-heated on a plane, and guard-heated on two planes sensors for 9 different Pe numbers in air.

Comparison of this plot with results calculated in water (Figure 4-10-c) indicates that the signal strength in air is lower than water, even though the thermal property of the fluid is considered in Pe number. In this circumstance, the thermal boundary layer is thick, which increases thermal capacity of the boundary layer and slows down normal heat diffusion and convection to the air. Deviation from the analytical solution is around 10% higher than when any of each designs is used for measurement in water at $Pe = 10,000$. This difference reduces to 5% at our lowest Pe number.

As mentioned, the low thermal conductivity of air leads to higher heat diffusion into the surroundings. Thus, the errors in single-element sensors such as spatial averaging are typically severe enough for measurements to be unacceptable— guard heating, if successful would yield high returns for this case. In order to quantitatively compare the heat distribution from the sensor, the equivalent length of each design is calculated based on the same amount of heat flux from the Leveque solution.
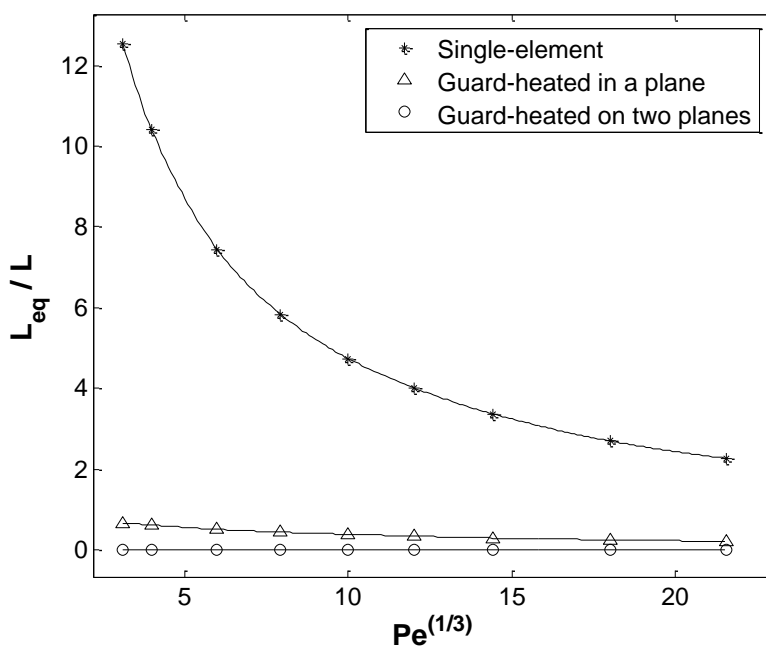
Figure 4-13 Upstream equivalent length (L$_{eq}$) per sensor length (L) of single-element, for sensing elements with guard-heating in a single plane, and on two planes. Sensors operate in air.

The upstream equivalent length for the single-element probe is more than 12 times the physical size of the sensor ($L = 24\mu$m) at $Pe = 30$. This ratio is about 17 times higher than the dimensionless equivalent length per sensor length when the fluid is water. Even though the trend of L_{eq}/L ratio shows a sharp drop at low Pe numbers, it is still twice as big as the sensor size at high Pe.

An interesting finding from the results in air and water is related to the guard-heated sensor on two planes in which the upstream equivalent length is trivial in both air and water. That is, the spatial averaging error, which is significant in the single-element sensor, is negligible when two supportive guard heaters surround the sensor.

Upstream L_{eq}/L ratio increases from 0.04 to 0.67 when the guard-heated sensor in a plane is applied in water and air, respectively, at low Pe numbers. For fast fluctuations, heat distribution against flow direction is negligible in both cases, as shown in the figure and Figure 4-11-b.
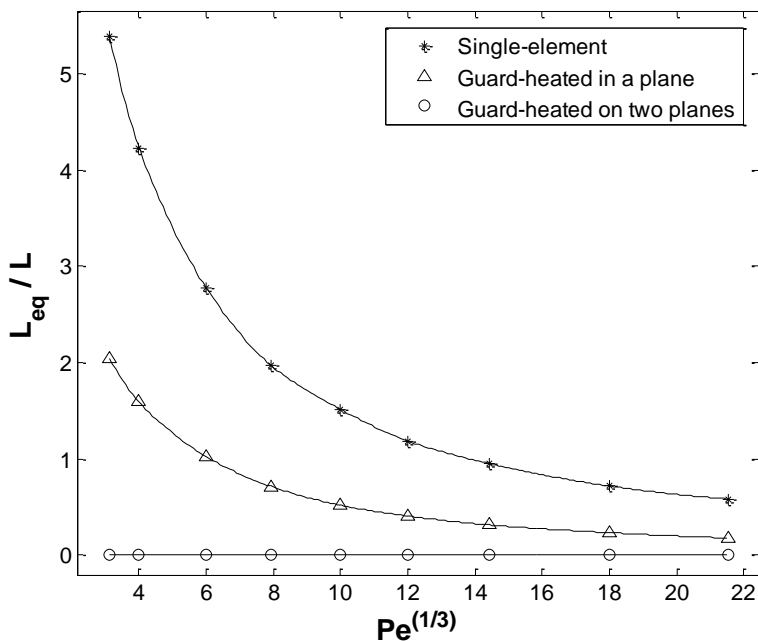
Figure 4-14- Downstream equivalent length (L_{eq}) per sensor length (L) of the single-element, guard-heated in a plane, and guard-heated on two planes sensors in air.

Downstream equivalent length also shows almost the same trend as in upstream. In general, the results shown in the air quantitatively show the problem is more severe for the single-element. We see that guard heating on two planes has less than 1% indirect

heat transfer, regardless of the fluid thermal properties. This design is thus an enabler for thermal WSS sensing in air, where the single element fares too poorly to be considered as a viable sensor.

4.5.2 Best location of the sensor in air within a guard-heater in a plane

Recall, one of our results was a suitable location of the sensor in the guard heater by finding the region where the ratio of direct to indirect heat transfer has a maximum value along the guard heater. As shown in Figure 4.4, this region does not move significantly depending on fluctuation magnitude. The following figure indicates the location movement is considerable when this type of sensor is used for measurement in air.

Figure 4-15- Undesirable indirect heat transfer from hot film, (Air-silica), x=0 and x=1 are the leading and trailing edges of the guard heater, respectively.

Therefore, the best performance of the sensor for measuring a wide range of fluctuations in air would diminish. Recall, the sensor position is fixed in the guard heater,

and cannot be moved during the experiment. So far, our results have shown a good control of indirect heat transfer by supporting the sensor with another heated film in a plane; although, movement of optimum location can be an issue in turbulent air flow. The question which arises here is if we are able to overcome this problem to some degree?

In the guard-heated sensor on two planes, indirect heat transfer is controlled effectively; thus, the effective sensor location movement is not an issue.

4.6. Temperature dependent fluid properties

So far, we have assumed that fluid thermal properties are independent from temperature for simplification. In this section, the influence of temperature on properties is considered. We have used the tabulated data for air and water in a range of temperature that the sensor is working at. It provided the constants of polynomial relation between temperature and air or water properties such as thermal diffusivity and viscosity. The non-dimensionalized rate of direct heat transfer from a single-element sensor ($L = 24\mu$m) with constant and temperature-dependent properties are shown in Figures 4-16.
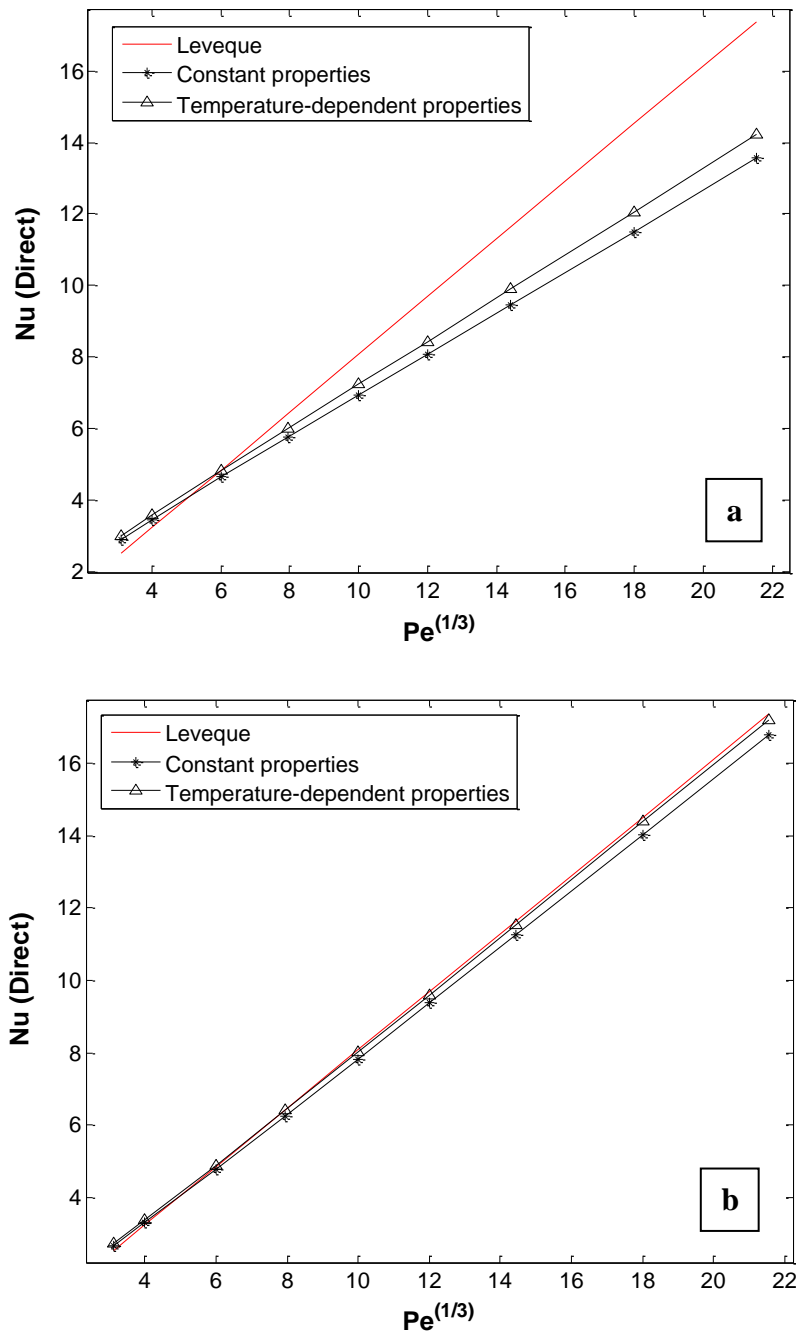
Figure 4-16- Non-dimensionalized direct heat transfer from the single-element sensor with constant and temperature-dependent properties a) in air b) in water.

Note that the difference between curves for two fluid properties is small and would not change the results significantly.

The last parameter we would like to study is the effect of substrate material. We chose silica for the substrate, as it has low thermal conductivity and suitable for fabrication. In the next section, we will compare silica with another material.

4.7. Two-layer substrate

Regardless of the geometrical design, the material used for the substrate should be taken into account. Two different materials, silicon and silica, are studied in this study in the interest of estimating the effect of wall thermal conductivity on the device. Silicon thermal conductivity, 148(W/m.K), is 107 times higher than silica, 1.38(W/m.K). In all previous results, silica (glass) was chosen as the substrate material. Fabricated guard-heated sensors explained in Chapter 3 are located on a silicon substrate; a thin layer of silicon dioxide sandwiched between the nickel film and silicon. In this section, the two-layer substrate made of silicon covered by 1μm silicon dioxide –5 times bigger than nickel film thickness– is computed. The question is does silica reduce the rate of heat loss to the substrate or the influence of preheating? Another question is whether the best location of the sensor within the plane guard heater moves depending on the substrate material?

First, conduction through the substrate was checked to estimate how the k_f/k_s ratio affects the best location of the sensor in the guard heater in a plane.
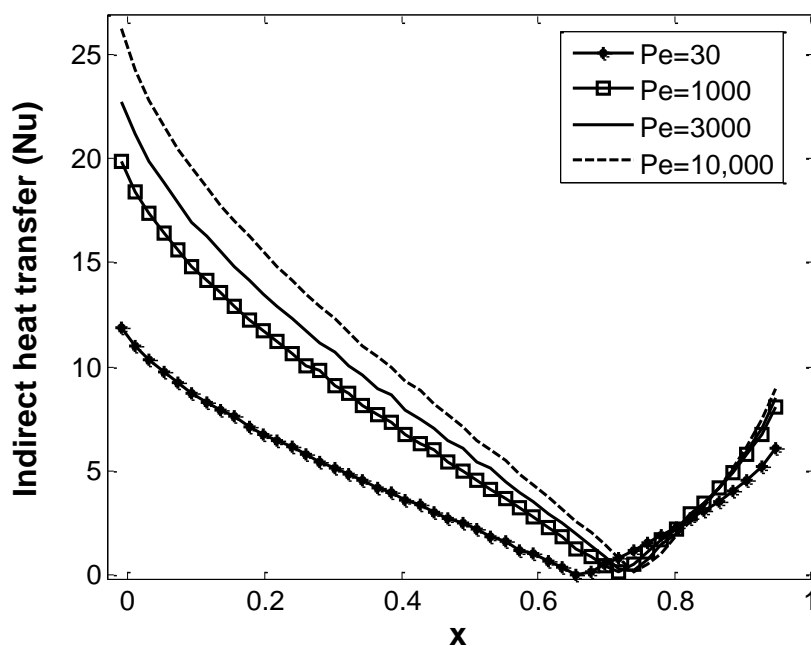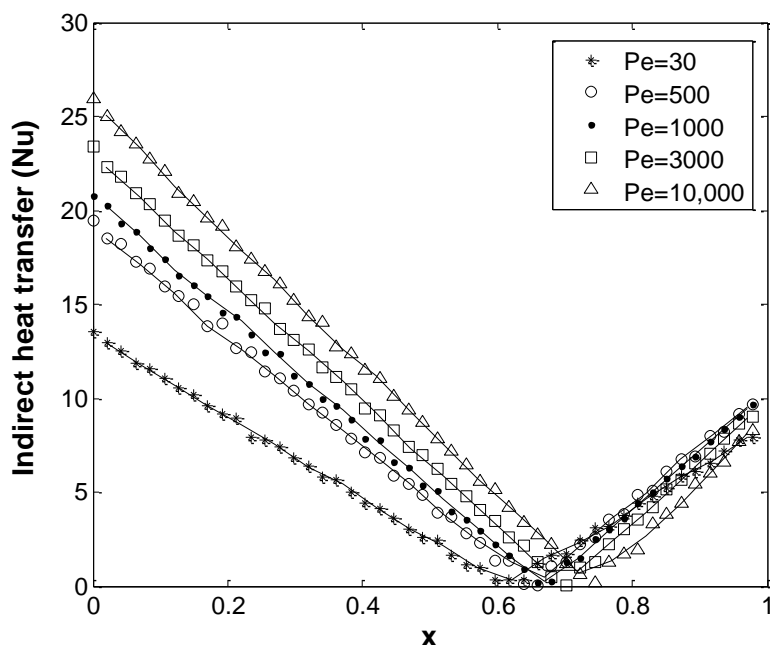
Figure 4-17- Undesirable indirect heat transfer from hot film, (silicon-silica-water), x=0 and x=1 are the leading and trailing edges of the guard heater, respectively.

The first undeniable change is the amount of indirect heat transfer through silicon which is considerably higher than silica, around 10 times higher. Therefore, the preheating term would not be trivial. The movement of best location of sensor toward upstream can be explained due to high thermal conductivity of silicon. As can be seen in the figure, appropriate material should be chosen in order to minimize indirect heat transfer in wide range of *Pe* numbers in measuring dynamic flow with the guard-heated sensor in plane.

Low direct heat transfer was estimated for a higher k_s/k_f as is expected according to Figure 7.a of Tardu [34].
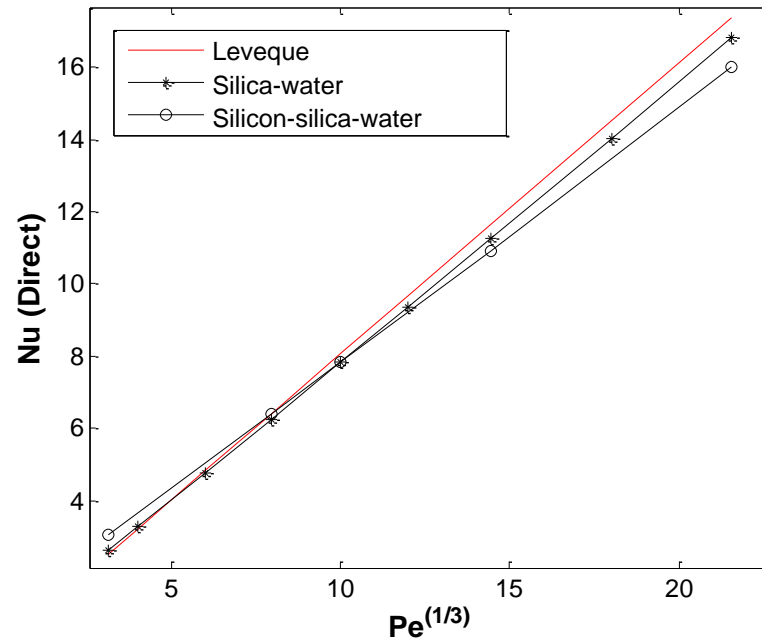
Figure 4-18- Non-dimensionalized direct heat transfer from single-element sensor for two cases: Silica-water and silicon-silica-water.

Our results show lower direct Nu numbers for the silicon-water case at high Pe numbers. The silica-water case also indicates stronger signals in addition to higher direct heat transfer. However, these differences are not very significant.

5. Conclusion and future work

5.1. Summary

Measurements for conventional, commercially available, single hot-film thermal sensors are not considered credible for wall shear stress fluctuation measurement over a wide range of flow Reynolds numbers, particularly in air. For such sensors, significant amount of heat diffusion to the substrate causes the sensor resolution to fluctuate with the quantity being measured and yields data with a spurious amplification at the low frequency end of the spectrum. As a check, our numerical simulations first verify the magnitudes of the errors reported in earlier published work.

Here we propose the concept of guard-heating, and use a detailed numerical study of two new designs, with guard heating elements on one plane and two planes. The overall contribution of this thesis is to show that errors of variable spatial averaging can be removed completely and low-frequency spectral distortion reduced significantly, by properly selecting geometric parameters for sensing and guard-heating elements. The specific main results of research in this thesis are listed below:

1) Our results prove the equivalent length of the guard-heated sensor on two planes matches the ideal –it is equal to the physical size of the sensor in any range of fluctuations. For the guard-heated sensors in a single plane, which are simpler to fabricate –the (Leveque) upstream equivalent length reduces from 12 times the sensing-element length to less than one sensor length in air (the ideal is zero).

2) The assumption that the mere presence of a guard heater will effectively block substrate conduction is shown to be incorrect. The best relative locations and sizes

for the sensing element within the guard heater affect the sensor accuracy in terms of decreasing the ratio of indirect to direct heat transfer. The numerical results in this thesis establish that there is a small region centered at 75% of the guard heater length from the leading edge (for water-silica; 65% for air-silica), in which this ratio approaches zero, as desired. For guard-heated sensors on two planes, there is low sensitivity to sensing element location within the top guard heater.

3) Since these sensing element locations within the guard heater bring the unwanted indirect substrate heat conduction to near zero, they are shown to be necessary and sufficient conditions for removal of the spurious variation of resolution with wall shear stress fluctuation magnitude. This makes these sensors suitable for measurements in turbulent flows with a large range of fluctuations.

4) The fraction of direct film-to-fluid heat transfer to the total heat generated in the sensing film for two sensor sizes ($L = 24\mu$m, $L = 2\mu$m) can be increased by around 10% in comparison to single-element, when a guard-heated sensor in a plane is applied in water. For the stronger fluctuations, substrate heat conduction can be reduced to 5% for a guard-heated sensor in a plane and below 1% with guard-heating on two planes.

5) The effect of temperature-dependent fluid properties on the transduction was investigated and found to require very modest correction.

6) Choice of substrate material plays an important role in the design. The amount of indirect heat transfer through silicon is considerably higher (about 10 times) than silica. In addition, the best location of the sensor within the guard heater changes

considerably with fluctuation strength, even in the case of water for a sensor built on a thin layer of thermal silicon oxide on top of a silicon wafer.

5.2. Recommendations for future work

All the results in this research are related to quasi-steady state situation, in which the time dependent term of wall shear stress is assumed to be zero. This assumption has been made to analyse the response of the sensor in respect to the wall shear stress of interest. This has allowed us to study a large range of design parameters in terms of steady substrate heat conduction reduction and allowed us to efficiently eliminate designs that would never work, even for the steady-state case. However, measurement in dynamic flows is the primary aim of thermal WSS sensors. In order to find a solution for time−dependent errors including spectral distortion of the sensor responses, time and phase lag and signal attenuation in fast fluctuations, unsteady conditions needs to be investigated.

An interesting possibility is to examine a different mode of operation, with transduction response to unsteady heating (periodic) of the sensing element, which can be explored numerically. By this means, the frequency used for generating heat in the sensor can be tuned depending on the range of magnitudes and time scales of the shear stress fluctuations, to improve the response of the sensor.

Bibliography

[1] Grosse, S. and Schroder, W., "wall-shear stress patterns of coherent structures in turbulent duct flow", *Journal of Fluid Mechanics*, 2009, **63**, pp. 147-158.

[2] Kasagi, N., Suzuki, Y. and Fukagata, K.," Microelectromechanical Systems–Based Feedback Control of Turbulence for Skin Friction Reduction" *Annual Review of Fluid Mechanics*, 2009, **41**, pp.231-251.

[3] Lofdahl, L. and Gad-el-Hak, M., "MEMS applications in turbulence and flow control". *Progress in Aerospace Sciences*, 1999, **35**, pp. 101-203.

[4] Iwamoto, K., Fukagata, K., Kasagi, N. and Suzuki, Y., "Friction drag reduction achievable by near-wall turbulence manipulation at high Reynolds number", *Physics of Fluids*, 2005, 17, Article number 011702.

[5] Iwamoto, K., Kasagi, N. and Suzuki, Y., "Dynamical roles of large-scale structures in turbulent channel flow", *Computational Mechanics*, 2004, MS022-174. Beijing: Tsinghua University.

[6] Acharya, M., Bornstein, J. and Escudier, M. P., "Development of a Floating Element for Measurement of Surface Shear Stress", *AIAA Journal*, 1985, **24**, pp. 410-415.

[7] Winter, K. G., "An Outline of the Techniques Available for the Measurement of Skin Friction", *Progress in Aerospace Sciences*, 1977, **18**, pp. 1-57.

[8] Goldstein, R. J., "Fluids Mechanics Measurements", *Taylor and Francis*, Philadelphia, 1996, 2nd Edition.

[9] Naughton, JW. and Sheplak, M., "Modern developments in shear-stress measurement", *Progress in Aerospace Sciences*, 2002, **38**, pp. 515–570.

[10] Chandrasekharan, V., Sells, J., Meloy, J., Arnold, DP. and Sheplak, M., "A Microscale Differential Capacitive Direct Wall-Shear-Stress Sensor", *Journal Of Microelectromechanical Systems*, 2011, **20**, pp. 622-635.

[11] Große, S. and Schroder, W., "Dynamic Wall-shear Stress Measurements in Turbulent Pipe Flow Using the Micro-pillar Sensor MPS[3]", *International Journal of Heat and Fluid Flow*, 2008, **29** (3), pp. 830–840.

[12] Nottebrock, B., Grobe, S., and Schroder, W., "Development of a Shear Stress Sensor to Analyse the Influence of Polymers on the Turbulent Wall Shear Stress", *Journal of physics: Condensed matter*, 2011, **23**, pp. 184121.

[13] Ayaz, UK., Loppolo, T. and Otugen, MV., "wall shear stress sensor based on the optical resonances of dielectric microspheres", *Journal of Measurement Science and Technology*, 2011, **22**, Article number 075203, 9pp.

[14] Mitchell, J. E. and Hanratty, T. J., "A Study of Turbulence at a Wall Using an Electrochemical Wall Shear-stress Meter", *The Journal of Fluid Mechanics*, 1966, **26**, pp. 199-221.

[15] Reiss, LP. and Hanratty, TJ., "An experimental study of the unsteady nature of the viscous sublayer", *AIChE Journal*, 1963, **9**, pp. 154-160.

[16] Leveque, M., "Leveque Leslois de la transmission de chaleur par convection", *Annus Mines Ser*, 1928, 12 (13), pp. 234‑242.

[17] Wagner, PM., "The use of near-wall hot-wire probes for time resolved skin-friction measurements", *In its Experimental Methods in Separated Flows (Technische University Berlin)*, 1991, pp. 524-529.

[18] Sturzebecher, D., Anders, S. and Nitsche, W., "The Surface Hot Wire as a Means of Measuring Mean and Fluctuating Wall Shear Stress", *Experiments in Fluids*, 2001, **31**, pp. 294-301.

[19] Alfredsson, P. H., Johansson, A.V., Haritonidis, J. H., Eckelmann, H., "The Fluctuating Wall Shear Stress and the Velocity Field in the Viscous Sublayer", *Physics of Fluids*, 1988, **31** (50), pp. 1026-1033.

[20] Chambers, F. W., Murohy, H. D. and McEligot, D. M., "Laterally converging flow. Part 1. Mean flow", *Journal of Fluid Mechanics*, 1982, **127**, pp. 379-403.

[21] Suzuki, Y. and Kasagi, N., "Evaluation of Hot-wire Measurements in Wall Shear Turbulence Using a Direct Numerical Simulation Database", *Experimental Thermal and Fluid Science*, 1992, **5**, pp. 69-77.

[22] Aoyagi, M., Takehana, N., Masuda, S. and Ariga, I., "Improvement of Hot Film Surface Gage for Wall Shear Stress Measurement", *Fluid control and measurement*, **2**, 1985, proceeding of the international symposium FLUCOME-85, Tokyo, pp. 863-868.

[23] Lin, Q., Jiang, F., Wang, X., Xu, Y., Han, Z., Tai, Y., Lew, J. and Ho, C. M., "Experiments and Simulations of MEMS Thermal Sensors for Wall Shear-stress Measurements in Aerodynamic Control Applications", *Journal of Micromechanics and Microengineering*, 2004, **14**, pp. 1640–1649.

[23] Yamagami, T., Suzuki, Y., and Kasagi, N., " Development of feedback control system of wall turbulence using MEMS devices*", Proceedings of 6th Symposium on Smart Control of Turbulence, Tokyo,* 2005, pp. 135-141.

[25] Bhiladvala, R. B., "Guard-Heated Thermal Sensor for Turbulent Wall-Shear Stress Fluctuations," The 20th International Symposium on Transport Phenomena, 2009, ISTP-20, Victoria, BC.

[26] Kalumuck, K., "A Theory for the Performance of Hot-film Shear Stress Probes", Ph.D. Thesis, MIT, 1983.

[27] Thomas, A. S. W., "Organised structures in the turbulent boundary layer", Ph.D. Thesis, University of Adelaide, 1977.

[28] Eckelmann, H., "The Structure of the Viscous sublayer and the Adjacent Wall Region in a Turbulent Channel Flow", *Journal of Fluid Mechanics*, 1974, **65** (3), pp. 439-459.

[29] Madavan, N. K., Deutsch, S. and Merkle, C. L., "Measurements of Local Skin Friction in a Microbubble-modified Turbulent Boundary Layer", *Journal of Fluid Mechanics*, 1985, **156**, pp. 237-256.

[30] Mao, Z., and Hanratty, T., "Application of an inverse mass transfer method to the measurement of turbulent fluctuations in the velocity gradient at the wall", *Experiments in Fluids*, 1991, **11**, pp. 65-73.

[31] Yoshino, T., Suzuki, Y. and Kasagi, N., "Assessment of the Wall Shear Stress Measurement with Arrayed Micro Hot-film Sensors in a Turbulent Channel Flow", *Proceeding of 2nd International Symposium on Turbulence and Shear Flow Phenomena*, 2001, **2**, pp. 153-158.

[32] Kim, J., Moin, P. and Moser, R., "Turbulence Statistics in Fully Developed Channel Flow at Low Reynolds Number", *Journal of Fluid Mechanics*, 1987, **177**, pp. 133-166.

[33] Dengel, P., Fernholz, H. H. and Hess, M. "Skin-friction Measurements in Two- and Three-dimensional Highly Turbulent Flows with Separation". *Advances in Turbulence, Proceedings of the First European* Turbulence Conference, 1987, pp. 470-479.

[34] Tardu, F. S. and Thanh Pham, C., "Response of Wall Hot-film Gages with Longitudinal Diffusion and Heat Conduction to the Substrate" *Journal of heat transfer*, 2005, **127**, pp. 812-819.

Appendix A
Leveque solution

Temperature field in the fluid can be described by the energy equation for incompressible, constant property flow:

$$\frac{\partial \theta}{\partial t} + u \frac{\partial \theta}{\partial x} + v \frac{\partial \theta}{\partial y} + w \frac{\partial \theta}{\partial z} = \alpha_f \left(\frac{\partial^2 \theta}{\partial x^2} + \frac{\partial^2 \theta}{\partial y^2} + \frac{\partial^2 \theta}{\partial z^2} \right)$$

Where θ is defined as non-dimensional temperature varied between zero and one.

$$\theta = \frac{(T - T_f)}{(T_w - T_f)}$$

T_w is the uniform temperature of the hot film maintained higher than its surrounding; T_f represents the fluid temperature not affected by the hot film. Heat transfer to the fluid happens along an infinite hot film.

Homogeneous flows with no viscous dissipation term are considered in this report. In order to simplify the case, some common assumptions can be made. First of all, the spanwise velocity fluctuation in comparison to streamwise fluctuation can be ignored. The fluctuation normal to the wall can also be ignored if the thermal boundary layer is in the region where v fluctuations are not significant. Natural convection is trivial compare to forced convection. Spanwise and streamwise conduction in the fluid can be neglected, as force convection is large.

Quasi-steady condition can be used if the time required for heat to diffuse and reach the thermal boundary layer thickness is less than the time takes for the current shear stress to pass the sensing element. In this circumstance, we can remove the time dependent term. Note that the problem is called quasi-steady, since the velocity gradient S_x is time dependent.

If the thermal boundary layer stays within the viscous sub layer- for all the shear stress ranges- $\bar{u}$ and $\acute{u}$ varies linearly with y. In this region, mean velocity and fluctuations are defined by $\bar{u} = \bar{s_x}y$ and $\acute{u} = \acute{s_x}y$, Where $s_x = \bar{s_x} + \acute{s_x}$ is velocity gradient at the wall. The shear stress is then $\tau_w = s_x\mu$; where μ is dynamic viscosity of the fluid.

Using these assumptions, the given equation is changed to the following relation:

$$s_x y \frac{\partial \theta}{\partial x} = \alpha_f \left(\frac{\partial^2 \theta}{\partial y^2}\right)$$

In order to obtain an ordinary differential equation, a similarity variable ($\eta = y(S_x/9\alpha x)^{1/3}$) was defined.

$$\frac{\partial^2 \theta}{\partial \eta^2} + 3\eta^2 \frac{\partial \theta}{\partial \eta} = 0$$

The boundary conditions for this equation are:

$$\begin{cases} \theta(\infty) = 1 \\ \theta(0) = 0 \end{cases}$$

The solution is

$$\theta(\eta) = \frac{\int_0^\eta e^{-r^3} dr}{\int_0^\infty e^{-r^3} dr} = \frac{1}{\Gamma(\frac{4}{3})} \int_0^\eta e^{-r^3} dr$$

To solve the ordinary differential equation, the integrals are evaluated numerically.

The heat transfer along the heating element is evaluated by the following relation

$$Q = \int_0^L K_f \left(\frac{\partial T}{\partial y}\right)_{y=0} W dx$$

Where K_f and W are fluid thermal conductivity and sensor width. The gradient $\left(\frac{\partial T}{\partial y}\right)_{y=0}$ is needed to be obtained.

$$\frac{\partial \theta}{\partial y} = \frac{\partial \theta}{\partial T} \frac{\partial T}{\partial y} = \frac{1}{(T_f - T_w)} \frac{\partial T}{\partial y}$$

$$\frac{\partial \theta}{\partial y} = \frac{\partial \theta}{\partial \eta} \frac{\partial \eta}{\partial y} = \frac{\partial \theta}{\partial \eta} (S_x/9\alpha x)^{1/3}$$

Thus,

$$\left(\frac{\partial T}{\partial y}\right)_{y=0} = \left(\frac{\partial \theta}{\partial \eta}\right)_{\eta=0} (S_x/9\alpha x)^{1/3} . (T_f - T_w)$$

The heat transfer rate can be rewrite as:

$$Q = (T_f - T_w) K_f W \left(\frac{\partial \theta}{\partial \eta}\right)_{\eta=0} \int_0^L \left(\frac{S_x}{9\alpha x}\right)^{\frac{1}{3}} dx$$

$$= (T_f - T_w)K_f W C_1 \left(\frac{S_x}{\alpha_f}\right)^{\frac{1}{3}} L^{2/3}$$

The constant of the integration and θ derivative $\left(\frac{\partial \theta}{\partial \eta}\right)_{\eta=0}$ are expressed as a constant

$C_1 = 0.807$.

The shear stress rate can be expressed by Pe number, $\left(\frac{S_x L^2}{\alpha_f}\right)$. Heat transfer rate can also be evaluated by $Q = hLW(T_f - T_w)$. Substituting Q and Pe number in the last equation gives the relation known as Leveque calibration relation:

$$Q = hLW(T_f - T_w) = (T_f - T_w)K_f W C_1 \left(\frac{S_x}{\alpha_f}\right)^{\frac{1}{3}} L^{2/3}$$

$$Nu = 0.807\, Pe^{1/3}$$

Where $Nu = hL/K_f$